JCP Online First, published on April 4, 2013 as 10.1136/jclinpath-2012-201431

Mitochondrial myopathy with autophagic vacuoles in patients with the m.8344A>G mutation

Jun-Hui Yuan, Yusuke Sakiyama, Itsuro Higuchi, Yukie Inamori, Yujiro Higuchi, Akihiro Hashiguchi, Keiko Higashi, Akiko Yoshimura, Hiroshi Takashima

▶ Additional material is published online only. To view please visit the journal online (http://dx.doi.org/10.1136/jclinpath-2012-201431).

Department of Neurology and Geriatrics, Kagoshima University, Graduate School of Medical and Dental Sciences, Kagoshima, Japan

Correspondence to
Dr Hiroshi Takashima, Department of Neurology and Geriatrics, Kagoshima University, Graduate School of Medical and Dental Sciences, 8-35-1 Sakuragaoka, Kagoshima City, Kagoshima 890-8520, Japan; thiroshi@m3.kufm.kagoshima-u.ac.jp

Received 28 December 2012
Accepted 11 March 2013

ABSTRACT

Background and aims In mitochondrial myopathy, autophagy is presumed to play an important role in mitochondrial dysfunction. Rimmed vacuoles (RVs), a sign of autophagy, can be seen as a secondary phenomenon in muscle ragged-red fibres (RRFs), whereas the uncommon presentation is that some fibres contain RVs, but without any mitochondrial abnormalities. To investigate the pathogenesis beneath this pathological phenomenon.

Methods We reviewed 783 skeletal muscle specimens and selected five obtained from patients with suspected mitochondrial myopathy, characterised by clearly visible autophagic vacuoles in non-RRFs, besides the coexistence of RRFs and cytochrome oxidase-negative fibres. Immunohistochemical staining with LC-3, and electron microscopy studies were performed. Using resequencing microarray and a next-generation sequencing system, the mitochondrial DNA was screened for mutations and the heteroplasmic level was measured in skeletal muscle and blood.

Results Muscle fibres with RVs and RRFs, as well as some morphologically normal fibres, stained strongly for LC-3. Electron microscopy disclosed significant abnormal mitochondrial proliferation and existence of autophagic vacuoles. After mutation screening, m.8344A>G in the $tRNA^{Lys}$ gene was detected in two patients. The heteroplasmy of mutated G was 45.1% in skeletal muscle and 17.8% in blood in patient 1; patient 2 exhibited 80.3% mutated G in skeletal muscle and 25.2% in blood.

Conclusions These findings demonstrate a new pathological phenotype for the m.8344A>G mutation-related disease and also provide pathological evidence of a correlation between mitochondrial abnormalities and autophagy.

INTRODUCTION

Autophagy generally has a cytoprotective function, often preceding cellular apoptosis or necrosis. Cellular vacuoles that contain fragments of cell components are called autophagic vacuoles. Rimmed vacuoles (RVs) are characterised by small vacuoles lined by many red granules (the 'rim'), as observed by modified Gomori trichrome (mGT) staining and contain fragments of cellular components, including membrane whorls, as observed under electron microscopy. The RVs represent a type of autophagic vacuole and are non-disease-specific structures found in various myopathies, particularly in hereditary inclusion body myopathy, distal myopathy with RVs and inclusion body myositis (IBM).[1] Autophagy also contributes to the degradation of mitochondria (mitophagy),[2] and dysfunctional mitochondria may trigger the activation of the autophagic pathway.[3]

Ragged-red fibres (RRF) are characterised by the existence of subsarcolemmal zones of bright red or reddish blue material in mGT stain (figure 1), which result from the accumulation of abnormal mitochondria beneath the sarcolemma of muscle fibres. Histochemical demonstration of RRFs and cytochrome c oxidase-negative fibres on muscle biopsy is considered to be the hallmark of a mitochondrial myopathy.[4] In our experience, RVs can be seen in the RRFs, as a secondary change of abnormal mitochondrial accumulation. On the other hand, it has been shown that frequent RRFs can be found in patients with IBM and may reflect an age-related decline in muscle mitochondrial oxidative metabolism.[5] Nevertheless, in five Japanese patients with suspected mitochondrial myopathy, we found that besides the prominent feature of RRFs, noticeable RVs appeared in the non-RRFs—an unexpected phenomenon.

m.8344A>G mutation in the $tRNA^{Lys}$ gene can result in a myoclonic epilepsy with RRF (MERRF syndrome) and is present in over 80% of affected subjects. Genetic analysis showed an m.8344A>G mutation in two of our patients. Typical MERRF syndrome is characterised by myoclonic epilepsy, cerebellar ataxia and RRFs in skeletal muscle tissue.[6] However, in this study, the phenotypes of the two patients with the m.8344A>G mutation were atypical; they had proximal muscle weakness and external ophthalmoplegia or preferential facioscapulohumeral muscle involvement.

We demonstrate a new pathological phenotype for the m.8344A>G mutation. These findings suggest a distinct pathogenesis between mitochondrial abnormalities and autophagy. The isolated autophagic vacuoles may also be associated with the atypical clinical phenotype of patients with an m.8344A>G mutation.

MATERIALS AND METHODS

Subjects

We examined 783 skeletal muscle specimens obtained from patients who were referred to our department between 2001 and 2011. Twenty-seven patients with definite coexistence of RRFs and RVs were selected, and then those with IBM (10 patients), dermatomyositis (three patients), polymyositis (one patient), amyotrophic lateral sclerosis (two patients), myotonic dystrophy (one patient) and non-specific myopathy (five patients) were excluded. Based on the clinical features, marked RRFs and cytochrome c oxidase-negative fibres in pathology, five Japanese patients with suspected

To cite: Yuan J-H, Sakiyama Y, Higuchi I, *et al*. *J Clin Pathol* Published Online First: [*please include* Day Month Year] doi:10.1136/jclinpath-2012-201431

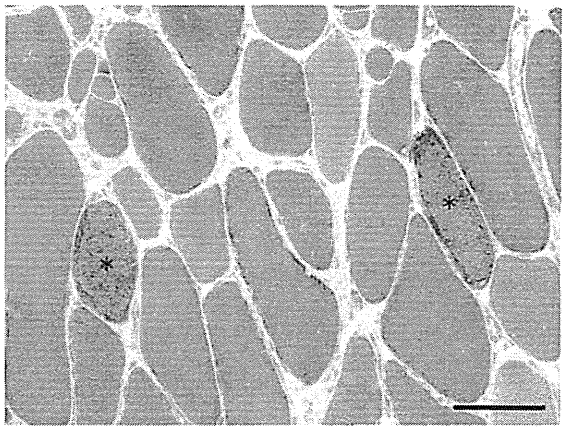

Figure 1 Modified Gomori trichrome staining of muscle ragged-red fibres (RRFs). RRFs are indicated by (*). Bar=100 μm.

mitochondrial myopathy were chosen for this study. Of these patients, only two who had the m.8344A>G mutation are described herein. No pathogenic mutation was detected in mtDNA from the other three patients. In addition, between 2001 and 2011, we identified the m.8344A>G mutation in blood from six of 169 patients with suspected mitochondrial disorders. Three of these patients underwent a muscle biopsy: two patients comprised the patients previously selected and the other exhibited a typical MERRF syndrome. However, because no definite RVs were seen in skeletal muscle, this last patient was excluded from the study.

All the diagnoses were made by experienced neurologists and pathologists based on clinical and laboratory examinations, electrobiological studies and skeletal muscle pathology.

Patient 1

A 51-year-old man with no family history of myopathy complained of general fatigue which he had had for 15 years. He began to experience muscle weakness from 36 years of age. This weakness gradually worsened, and by the age of 40 years he had difficulty in walking. Over the following 3 years, the symptoms progressed until he was incapable of lifting any substantial weight. Physical examination showed moderate muscle weakness in the facial, cervical and proximal muscles. His eye movements were also restricted in the superoinferior direction and he had difficulty hearing high-pitched voices. His serum creatine kinase level was raised at 1378 U/l (normal range 45–163 U/l).

Patient 2

A 54-year-old man reported a 24-year history of muscle weakness; there was no family history of any such difficulty. At 30 years of age, he experienced difficulty in lifting his arms and his cervical muscles gradually became affected. He occasionally tumbled down staircases; one fall required admission to hospital for a subarachnoid haemorrhage. Physical examination at the time of study enrolment showed marked weakness and wasting of the shoulder girdle muscles, without scapular winging. The facial muscles, intrinsic muscles of the hand and thigh muscles were also found to be atrophied. The extraocular muscles and the cranial nerves were normal and no other abnormalities were detected. His serum creatine kinase level was 46 U/l. CT indicated myoatrophy in his arms.

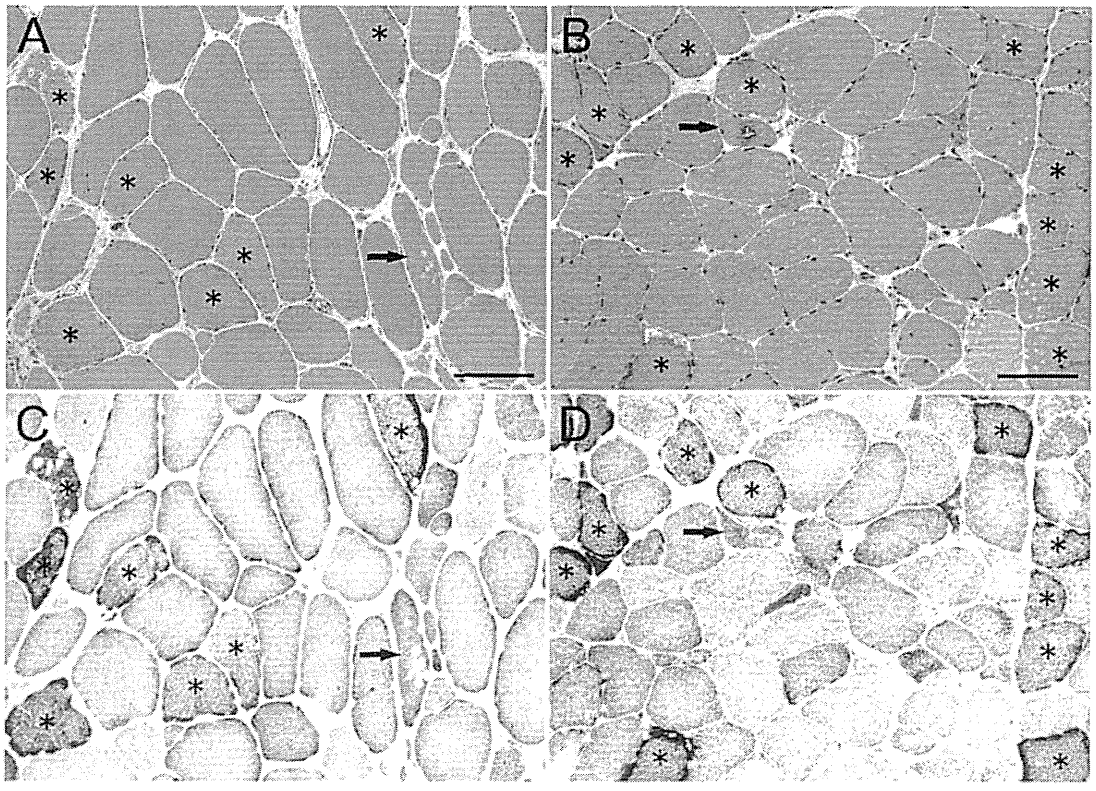

Figure 2 Histochemical staining of muscle ragged-red fibres (RRFs) and isolated rimmed vacuoles in patient 1 (A and C) and patient 2 (B and D). Haematoxylin and eosin (A and B) and succinate dehydrogenase (C and D) staining shows numerous RRFs (*), coexisting with non-RRFs containing rimmed vacuoles (arrow). Bar=100 μm.

We carried out a neurological examination and neuroradiological study in both patients and no comorbidities, including vascular disease, were seen, except for traumatic subarachnoid haemorrhage in patient 2.

Pathological studies

Skeletal muscle samples were obtained from the biceps brachii. Serial frozen sections (8 μm) were prepared and stained with multiple histochemical methods (see online supplementary table 1).

Other sections prepared on aminosilane-coated slides were immunohistochemically stained with 1:50 diluted microtubule-associated protein 1 light chain 3B (LC-3) clone 5F10 (Nano Tools, France). Biotinylated anti-mouse IgG was used as the secondary antibody and the avidin–biotin–peroxidase complex (ABC) method was used for signal detection (ABC kit; Vector Laboratories, Burlingame, California, USA). All the immunohistochemical procedures were performed as reported previously.[7]

A small amount of the muscle specimens was fixed in glutaraldehyde in cacodylate buffer, post-fixed in 1% buffered osmium tetroxide and then embedded in Epon. Semi-thin sections were prepared for light microscopy to localise the target region, while ultra-thin sections were cut and stained with uranyl acetate and lead citrate for electron microscopy. The electron microscopy procedures were performed as described previously.[8]

Mitochondrial DNA analysis

Genome DNA was extracted from both peripheral blood leucocytes (Qiagen, Maryland, USA) and frozen muscle specimens using a DNeasy blood and tissue kit (Qiagen). The entire mitochondrial DNA extracted from the skeletal muscles was sequenced using MitoChip V.2.0 (GeneChip Human Mitochondrial Resequencing Array 2.0) and analysed on GeneChip Sequence Analysis Software V.4.0.[9 10] Previously described primers were used,[11] and the variations detected by MitoChip V.2.0 were then confirmed by direct Sanger sequencing, as described.[12]

The polymorphic and pathogenic natures of the confirmed mutations were checked against two databases: MITOMAP (http://www.mitomap.org/) and GiiB-JST mtSNP (http://mtsnp.tmig.or.jp/mtsnp/index.shtml).

Heteroplasmic study

The GS Junior platform can sequence 1 00 000 single PCR fragments in parallel, which enables the detection of low levels of mtDNA heteroplasmy.[13 14] Using the Primer 3 program, we designed oligonucleotide primers flanking the m.8344A>G mutation (forward: 5′-CACTTTCACCGCTACACGAC-3′ and reverse: 5′-GCAATGAATGAAGCGAACAG-3′), which will generate a 428 bp PCR product. Using 50 ng genomic DNA from both blood and skeletal muscle of the two patients, after hot-start PCR, the products were sequenced on the GS Junior platform (Roche-454 Life Sciences, Basel, Switzerland) in accordance with the manufacturer's protocol. The results were assembled using the reference sequence (NC_012920) and analysed using GS Reference Mapper (454 Life Science) software.[15]

RESULTS

Pathological studies

In patients, histopathology showed moderate variation in muscle fibre size; numerous degenerating fibres with occasional regenerating or necrotic fibres were seen. RRFs were detected in 12.4% of muscle fibres (497/4001) in patient 1 and 20.7% of muscle fibres (253/1220) in patient 2. RVs were seen in occasional non-RRFs (figure 2). Cytochrome c oxidase activity was significantly decreased or absent in many fibres, particularly the RRFs, in which high succinate dehydrogenase expression was observed. The cytochrome c oxidase activity was increased in the non-RRF fibres containing isolated RVs. No blood vessels were seen that showed strong succinate dehydrogenase reactivity. Muscle fibres with RVs and RRFs, as well as some morphologically normal fibres, stained strongly for LC-3 (figure 3).

Electron microscopy in the biopsied muscle of the two patients disclosed significant abnormal mitochondrial proliferation with paracrystalline inclusions and circular arrangements of cristae. Autophagic vacuoles with membranous whorls and myelin-like structures were also seen (figure 4).

Mitochondrial DNA analysis

Using MitoChip V.2.0, 57 mitochondrial DNA variations were detected in skeletal muscle samples from the two patients and 54 were confirmed to be single nucleotide polymorphisms (SNPs) by referring to the MITOMAP and GiiB-JST mtSNP databases. An m.8344A>G mutation in the $tRNA^{Lys}$ gene was detected in both patients and subsequently confirmed by direct sequencing of DNA from both muscle and blood lymphocytes (figure 5). In addition, a new SNP, m.306C>A in the non-coding area and a missense mutation m.3433T>A (Tyr43Asp) in the ND1 gene of patient 2 were also found. However, considering the vital role of the $tRNA^{Lys}$ gene, we considered m.8344A>G to be the causative mutation.

Heteroplasmic study

Using the GS Junior platform, we clonally amplified and read more than 100 copies of each original amplicon from blood and muscle, in both patients. The percentage of 8344G in patient 1 was 17.8% (23/129) in blood and 45.1% (142/315) in muscle. In patient 2, the percentage was 25.2% (81/321) in blood and 80.3% (598/745) in muscle (figure 5).

DISCUSSION

We selected five patients with suspected mitochondrial myopathy and characterised by the coexistence of RRFs and isolated RVs in muscle fibres. Using a resequencing microarray and a next-generation sequencing system, we identified both the m.8344A>G mutation and its heteroplasmic nature in two of these patients.

m.8344A>G, with a prevalence rate of no more than 0.25/100 000 in Europe, is the most common mutation of MERRF syndrome.[16–18] The clinical variations of MERRF syndrome are extensively expanded to encephalitis, infantile putaminal necrosis, depression, Parkinson's disease, cardiomyopathy, neuropathy, ophthalmoplegia, chronic pancreatitis and the MELAS phenotype that comprises mitochondrial encephalomyopathy, lactic acidosis and stroke-like episodes.[19–26] In our study, patient 1 had progressive proximal muscle weakness, restriction of superoinferior eye movement and hearing loss. Patient 2 experienced isolated skeletal muscle effects, with involvement of the facial and proximal upper limb muscles. Although they harboured the MERRF mutation, both patients presented with nearly isolated myopathy rather than the typical MERRF syndrome with myoclonus epilepsy or cerebellar ataxia.

RRFs formed the predominant pathological feature in 12.4% and 20.7% of fibres in patients 1 and 2, respectively. The combination of cytochrome c oxidase-negative fibres and abnormally proliferated mitochondria found in electron microscopy, confirmed the pathological diagnosis of mitochondrial myopathy. In both patients haematoxylin and eosin and mGT staining

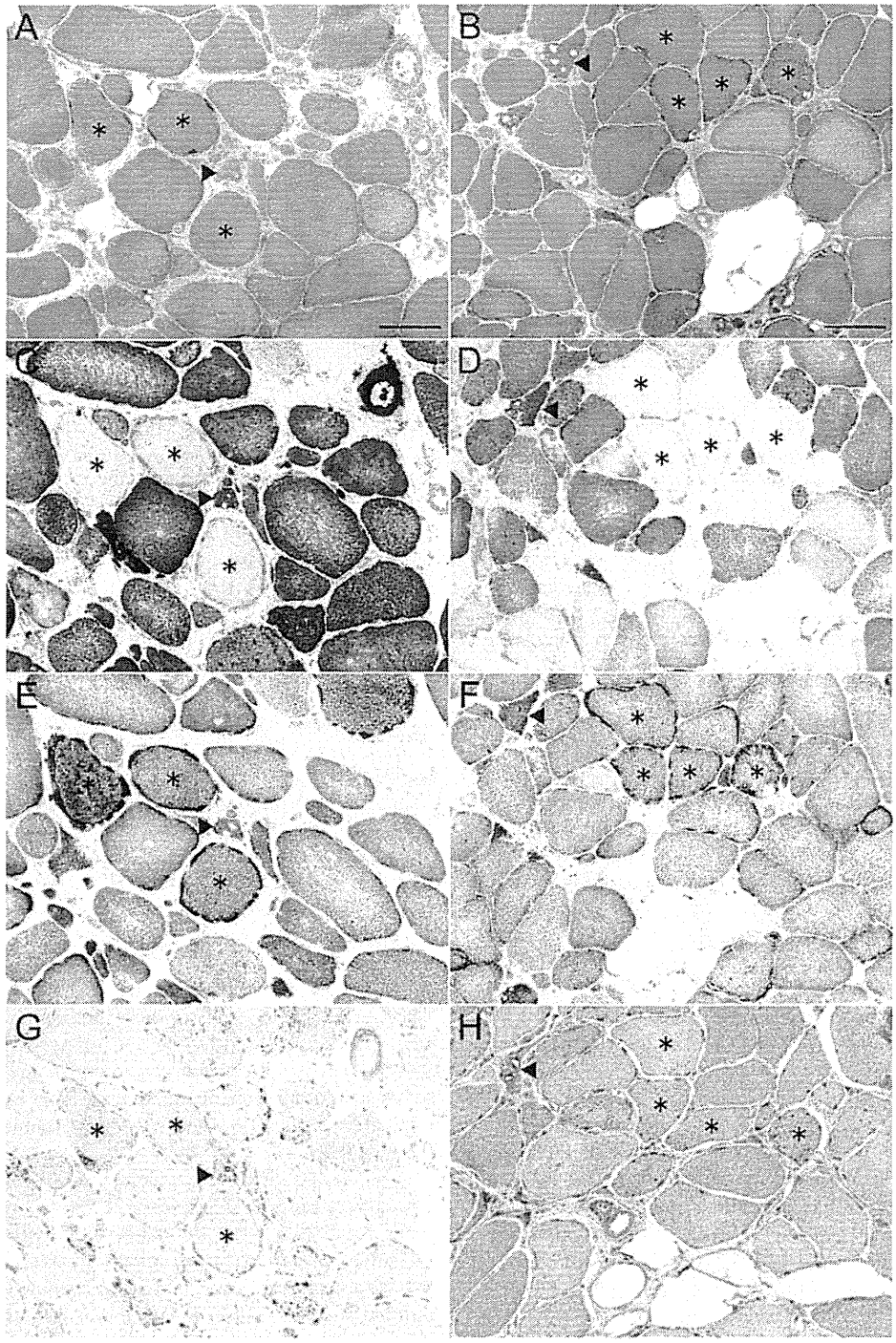

Figure 3 Serial sections of histochemical and immunohistochemical stained skeletal muscle samples in patient 1 (A, C, E and G) and patient 2 (B, D, F and H). Moderate myopathic change with coexistence of numerous in muscle ragged-red fibres (RRFs) (*) and some rimmed vacuoles (▲) is seen with the modified Gomori trichrome stain (A and B). Cytochrome c oxidase activity is significantly decreased or absent in many fibres, particularly RRFs (C and D), with high succinate dehydrogenase expression (E and F). Immunohistochemical staining of LC-3 was strong in fibres with rimmed vacuoles and RRFs and also in some morphologically normal fibres (G and H). Bar=100 μm.

demonstrated RVs in fibres without mitochondrial accumulation or loss of cytochrome c oxidase activity. LC-3 aggregation was seen in fibres with isolated RVs, RRFs with secondary vacuolation and even in some fibres without any morphological changes. These abnormalities suggest the overexpression of autophagy or disorders of autophagic pathways in these fibres.[27] Electron microscopy also confirmed the existence of autophagic vacuoles. Although mild autophagic changes can be seen in RRFs of patients with common mitochondrial myopathies, conspicuous RVs and LC3-positive fibres in non-RRFs were the characteristic findings in both of our study patients. Additionally, degeneration, regeneration or necrosis of muscle fibres indicated active cellular damage, probably resulting from mitochondrial dysfunction.

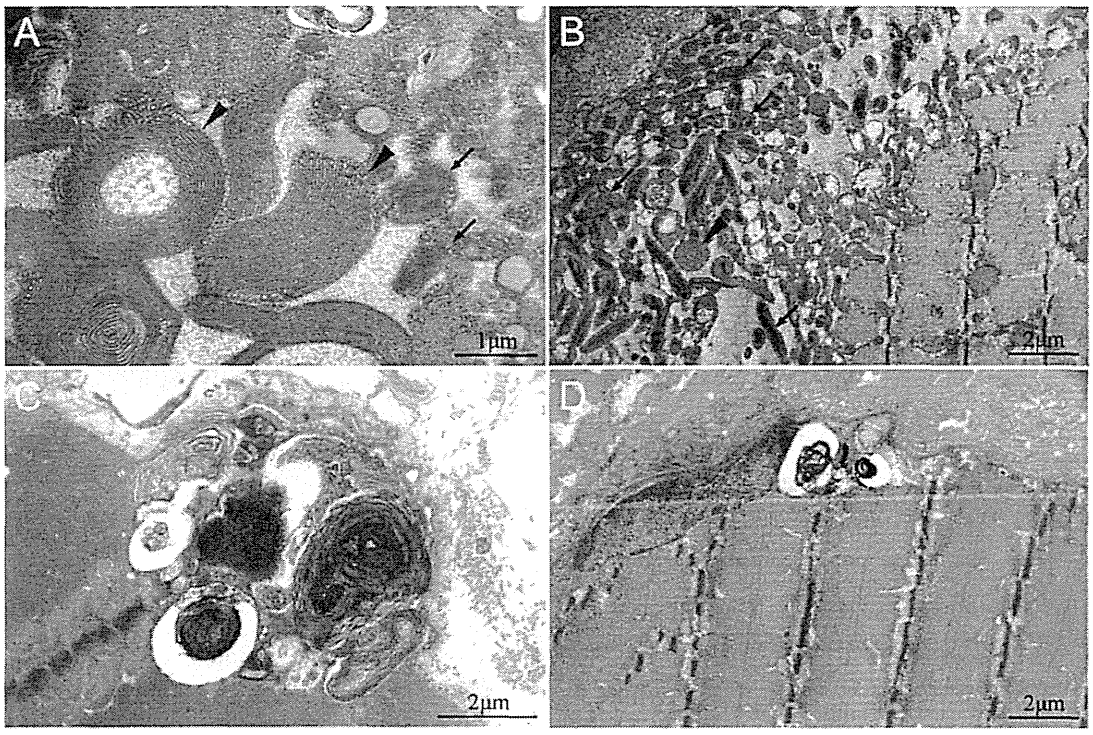

Figure 4 Electron microscopy of abnormal mitochondria and autophagic vacuoles in skeletal muscle tissue from patient 1 (A and C) and patient 2 (B and D). Significant abnormal mitochondrial proliferation is seen, with paracrystalline inclusions (↙) and circular arrangements of cristae (▲) (A and B). Some autophagic vacuoles have membranous whorls and myelin-like structures (C and D).

It has been reported that the $tRNA^{Lys}$ gene with the m.8344A>G mutation particularly lacks post-transcriptional modification of uridine at the first letter of the anticodon (the wobble position)[28]; mutant tRNAs without the wobble modification cannot fulfil their normal role as acceptor molecules in the translation process, which results in respiratory chain defects and also in impaired global protein synthesis and compromised mitochondrial translation products.[29 30] Cells with the m.8344A>G mutation were recently shown to have increased autophagic activity.[31] We therefore postulate that the singular devastating effect of the m.8344A>G mutation in the $tRNA^{Lys}$ gene is to induce active autophagy for the purpose of abnormal mitochondria removal.

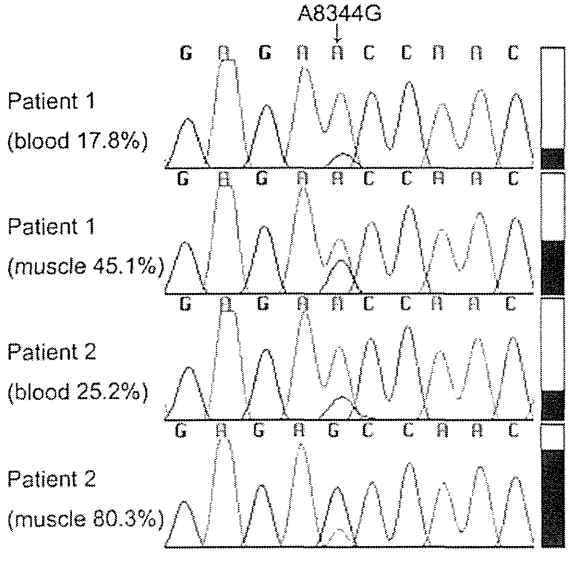

Figure 5 Sequence chromatograms and block diagrams of m.8344A>G mutation heteroplasmy in both blood and skeletal muscle DNA from the two patients. The mutation rate in blood and skeletal muscle was 17.8% and 45.1% in patient 1, respectively, and 25.2% and 80.3%, respectively, in patient 2. The arrow indicates the mutation site.

Mutations in mtDNA including m.8344A>G are always heteroplasmic, meaning that mutant and wild-type genomes coexist. The autophagic targeting of mitochondria adds to this heterogeneity.[32] The threshold for biochemical expression of a mtDNA mutation varies, depending on the mutation and the tissue involved. In the muscle fibres containing isolated RVs, the heteroplasmy of mutated G may be below the threshold required to cause a RRF, but trigger the autophagy pathway first. The GS Junior platform was used to confirm the heteroplasmy of 8344G, and the relatively low heteroplasmy level in blood may explain the predominantly skeletal muscle phenotype seen in the two patients. We recommend that patients suspected of having a mitochondrial disorder undergo genetic analysis of mtDNA, using muscle as the preferred tissue type.

In summary, we focused on a rare pathological phenomenon of coexistence of RRFs and isolated RVs, and identified the m.8344A>G mutation in two patients with atypical MERRF syndrome. This finding suggests that the distinctive pathogenesis results from the m.8344A>G mutation in both patients. The autophagy, always considered to be a secondary process after mitochondrial dysfunction, may work earlier than expected. Although the mechanism of detailed interaction between the m.8344A>G mutation and autophagy requires further investigation, these findings broaden the pathological phenotype of patients with the m.8344A>G mutation.

Take-home messages

- The interaction between autophagy and mitochondrial dysfunction remains unclear. The finding of isolated autophagic vacuoles in muscle fibres of patients with the m.8344A>G mutation, might be a starting point.
- The autophagic vacuoles, found in muscle fibres, might be associated with the atypical phenotype for a m.8344A>G mutation.
- The next-generation sequencing system might be reliable for detecting the heteroplasmy level of a mitochondrial DNA mutation.

Acknowledgements The authors thank N Hirata and Y Shirahama of our department for their excellent technical assistance. We also wish to thank the Joint Research Laboratory, Kagoshima University Graduate School of Medical and Dental Sciences for the use of their facilities.

Contributors J-HY carried out genetic experiments and drafted the manuscript. YS, YH and AY participated in genetic experiments and revised the manuscript. IH designed the study, revised the manuscript and obtained funding. YI, KH and AH carried out pathological and electron microscopy study. HT designed and supervised the study, revised the manuscript and obtained funding.

Funding The project was funded by the Ministry of Education, Culture, Sports, Science and Technology of Japan (grant 21591095 to HT; 21591094 to IH), intramural research grant (21B-1 to IH) for neurological and psychiatric disorders of the National Center of Neurology and Psychiatry, the Nervous and Mental Disorders and Research Committee for Charcot-Marie-Tooth disease, neuropathy, ataxic disease and applied health and technology of the Ministry of Health, Welfare and Labour, Japan and a research grant (23300201) from the Ministry of Health, Labour and Welfare of Japan.

Competing interests None.

Ethics approval Institutional review board of Kagoshima University.

Provenance and peer review Commissioned; externally peer reviewed.

REFERENCES

1 Kumamoto T, Ueyama H, Tsumura H, *et al*. Expression of lysosome-related proteins and genes in the skeletal muscles of inclusion body myositis. *Acta Neuropathol* 2004;107:59–65.
2 Kim I, Rodriguez-Enriquez S, Lemasters JJ. Selective degradation of mitochondria by mitophagy. *Arch Biochem Biophys* 2007;462:245–53.
3 Geisler S, Holmström KM, Skujat D, *et al*. PINK1/Parkin-mediated mitophagy is dependent on VDAC1 and p62/SQSTM1. *Nat Cell Biol* 2010;12:119–31.
4 DiMauro S, Hirano M, Kaufmann P, *et al*. Clinical features and genetics of myoclonic epilepsy with ragged red fibers. *Adv Neurol* 2002;89:217–29.
5 Rifai Z, Welle S, Kamp C, *et al*. Ragged red fibers in normal aging and inflammatory myopathy. *Ann Neurol* 1995;37:24–9.
6 Shoffner JM, Lott MT, Lezza AM, *et al*. Myoclonic epilepsy and ragged-red fiber disease (MERRF) is associated with a mitochondrial DNA tRNA(Lys) mutation. *Cell* 1990;61:931–7.
7 Higuchi I, Niiyama T, Uchida Y, *et al*. Multiple episodes of thrombosis in a patient with Becker muscular dystrophy with marked expression of utrophin on the muscle cell membrane. *Acta Neuropathol* 1999;98:313–16.
8 Niiyama T, Higuchi I, Suehara M, *et al*. Electron microscopic abnormalities of skeletal muscle in patients with collagen VI deficiency in Ullrich's disease. *Acta Neuropathol* 2002;104:67–71.
9 Zhou S, Kassauei K, Cutler DJ, *et al*. An oligonucleotide microarray for high-throughput sequencing of the mitochondrial genome. *J Mol Diagn* 2006;8:476–82.
10 Mithani SK, Smith IM, Zhou S, *et al*. Mitochondrial resequencing arrays detect tumor-specific mutations in salivary rinses of patients with head and neck cancer. *Clin Cancer Res* 2007;13:7335–40.
11 Rieder MJ, Taylor SL, Tobe VO, *et al*. Automating the identification of DNA variations using quality-based fluorescence re-sequencing: analysis of the human mitochondrial genome. *Nucleic Acids Res* 1998;26:967–73.
12 Sakiyama Y, Okamoto Y, Higuchi I, *et al*. A new phenotype of mitochondrial disease characterized by familial late-onset predominant axial myopathy and encephalopathy. *Acta Neuropathol* 2011;121:775–83.
13 Li M, Schönberg A, Schaefer M, *et al*. Detecting heteroplasmy from high-throughput sequencing of complete human mitochondrial DNA genomes. *Am J Hum Genet* 2010;87:237–49.
14 Tang S, Huang T. Characterization of mitochondrial DNA heteroplasmy using a parallel sequencing system. *Biotechniques* 2010;48:287–96.
15 Holland MM, McQuillan MR, O'Hanlon KA. Second generation sequencing allows for mtDNA mixture deconvolution and high resolution detection of heteroplasmy. *Croat Med J* 2011;52:299–313.
16 Chinnery PF, Johnson MA, Wardell TM, *et al*. The epidemiology of pathogenic mitochondrial DNA mutations. *Ann Neurol* 2000;48:188–93.
17 Darin N, Oldfors A, Moslemi AR, *et al*. The incidence of mitochondrial encephalomyopathies in childhood: clinical features and morphological, biochemical and DNA abnormalities. *Ann Neurol* 2001;49:377–83.
18 Remes AM, Majamaa-Voltti K, Kärppä M, *et al*. Prevalence of large-scale mitochondrial DNA deletions in an adult Finnish population. *Neurology* 2005;64:976–81.
19 Orcesi S, Gorni K, Termine C, *et al*. Bilateral putaminal necrosis associated with the mitochondrial DNA A8344G myoclonus epilepsy with ragged red fibers (MERRF) mutation: an infantile case. *J Child Neurol* 2006;21:79–82.
20 Molnar MJ, Perenyi J, Siska E, *et al*. The typical MERRF (A8344G) mutation of the mitochondrial DNA associated with depressive mood disorders. *J Neurol* 2009;256:264–5.
21 Horvath R, Kley RA, Lochmuller H, *et al*. Parkinson syndrome, neuropathy and myopathy caused by the mutation A8344G (MERRF) in tRNALys. *Neurology* 2007;68:56–8.
22 Vallance HD, Jeven G, Wallace DC, *et al*. A case of sporadic infantile histiocytoid cardiomyopathy caused by the A8344G (MERRF) mitochondrial DNA mutation. *Pediatr Cardiol* 2004;25:538–40.
23 Erol I, Alehan F, Horvath R, *et al*. Demyelinating disease of central and peripheral nervous systems associated with a A8344G mutation in tRNALys. *Neuromuscul Disord* 2009;19:275–8.
24 Naini AB, Lu J, Kaufmann P, *et al*. Novel mitochondrial DNA ND5 mutation in a patient with clinical features of MELAS and MERRF. *Arch Neurol* 2005;62:473–6.
25 Nishigaki Y, Tadesse S, Bonilla E, *et al*. A novel mitochondrial tRNA(Leu(UUR)) mutation in a patient with features of MERRF and Kearns-Sayre syndrome. *Neuromuscul Disord* 2003;13:334–40.
26 Toyono M, Nakano K, Kiuchi M, *et al*. A case of MERRF associated with chronic pancreatitis. *Neuromuscul Disord* 2001;11:300–4.
27 Kuma A, Matsui M, Mizushima N. LC3, an autophagosome marker, can be incorporated into protein aggregates independent of autophagy: caution in the interpretation of LC3 localization. *Autophagy* 2007;3:323–8.
28 Yasukawa T, Suzuki T, Ishii N, *et al*. Defect in modification at the anticodon wobble nucleotide of mitochondrial tRNA(Lys) with the MERRF encephalomyopathy pathogenic mutation. *FEBS Lett* 2000;467:175–8.
29 Masucci JP, Schon EA, King MP. Point mutations in the mitochondrial tRNA(Lys) gene: implications for pathogenesis and mechanism. *Mol Cell Biochem* 1997;174:215–19.
30 Yasukawa T, Suzuki T, Ishii N, *et al*. Wobble modification defect in tRNA disturbs codon-anticodon interaction in a mitochondrial disease. *EMBO J* 2001;20:4794–802.
31 Chen CY, Chen HF, Gi SJ, *et al*. Decreased heat shock protein 27 expression and altered autophagy in human cells harboring A8344G mitochondrial DNA mutation. *Mitochondrion* 2011;11:739–49.
32 Wikstrom JD, Twig G, Shirihai OS. What can mitochondrial heterogeneity tell us about mitochondrial dynamics and autophagy? *Int J Biochem Cell Biol* 2009;41:1914–27.

Journal of the Peripheral Nervous System 18:89–93 (2013)

CASE REPORT

Novel mutation in the replication focus targeting sequence domain of *DNMT1* causes hereditary sensory and autonomic neuropathy IE

Junhui Yuan[1], Yujiro Higuchi[1], Tatsui Nagado[2], Satoshi Nozuma[1], Tomonori Nakamura[1], Eiji Matsuura[1], Akihiro Hashiguchi[1], Yusuke Sakiyama[1], Akiko Yoshimura[1], and Hiroshi Takashima[1]

[1] *Department of Neurology and Geriatrics, Kagoshima University, Graduate School of Medical and Dental Sciences; and* [2] *Department of Neurology, Imakiire General Hospital, Kagoshima, Japan*

Abstract *DNMT1*, encoding DNA methyltransferase 1 (Dnmt1), is a critical enzyme which is mainly responsible for conversion of unmethylated DNA into hemimethylated DNA. To date, two phenotypes produced by *DNMT1* mutations have been reported, including hereditary sensory and autonomic neuropathy (HSAN) type IE with mutations in exon 20, and autosomal dominant cerebellar ataxia, deafness, and narcolepsy caused by mutations in exon 21. We report a sporadic case in a Japanese patient with loss of pain and vibration sense, chronic osteomyelitis, autonomic system dysfunctions, hearing loss, and mild dementia, but without definite cerebellar ataxia. Electrophysiological studies revealed absent sensory nerve action potential with nearly normal motor nerve conduction studies. Brain magnetic resonance imaging revealed mild diffuse cerebral and cerebellar atrophy. Using a next-generation sequencing system, 16 candidate genes were analyzed and a novel missense mutation, c.1706A>G (p.His569Arg), was identified in exon 21 of *DNMT1*. Our findings suggest that mutation in exon 21 of *DNMT1* may also produce a HSAN phenotype. Because all reported mutations of *DNMT1* are concentrated in exons 20 and 21, which encode the replication focus targeting sequence (RFTS) domain of Dnmt1, the RFTS domain could be a mutation hot spot.

Key words: DNA methyltransferase 1, *DNMT1*, hereditary sensory and autonomic neuropathy, missense mutation, next-generation sequencing

Introduction

DNA methyltransferase 1 (Dnmt1), encoded by *DNMT1*, is the principal enzyme responsible for the maintenance of cytosine methylation at cytosine–phosphate–guanine dinucleotides in the mammalian genome *(Feng and Fan, 2009)*, and is also crucial for gene regulation and chromatin stability *(Tohgi et al., 1999; Chen et al., 2003)*. Human Dnmt1 consists of a conserved C-terminal catalytic core and a large N-terminal region harboring multiple globular conserved domains, including the DNA methyltransferase-associated protein 1-binding domain, the proliferating cell nuclear antigen-binding domain, the replication focus targeting sequence (RFTS) domain, the CXXC domain, and two bromo-adjacent homology domains *(Syeda et al., 2011)*.

To date, eight kindreds with *DNMT1* mutations have been reported, half of which were characterized

Address correspondence to: Prof. Hiroshi Takashima, Department of Neurology and Geriatrics, Kagoshima University, Graduate School of Medical and Dental Sciences, 8-35-1 Sakuragaoka, Kagoshima City, Kagoshima 890-8520, Japan. Tel: +(81)99-275-5330; Fax: +(81)99-265-7164; E-mail: thiroshi@m3.kufm.kagoshima-u.ac.jp

by sensory neuropathy, sensorineural hearing loss, and dementia, caused by mutations in exon 20 *(Klein et al., 2011)*; the other half presented with autosomal dominant cerebellar ataxia, deafness, and narcolepsy, and all mutations were located in exon 21 *(Winkelmann et al., 2012)*. It is noteworthy that all peptides coded by exon 20 and 21 belong to the RFTS domain of Dnmt1.

Using a next-generation sequencing (NGS) system, we screened a panel of candidate genes in a Japanese patient with sensory neuropathy, autonomic nervous system dysfunctions, sensorineural hearing loss, and slight dementia. This screen identified a novel missense mutation in exon 21 of *DNMT1*. We also reviewed all reported cases with *DNMT1* mutation and investigated the pathogenesis of various *DNMT1*-related phenotypes.

Case Report

The patient was a 41-year-old Japanese male from a non-consanguineous family (Fig. 1A). No neurological disorders were found in other family members. Pain perception began to decrease in his distal lower limbs after high school, and this condition progressed slowly. At the age of 30 and 32, after local infection, he had osteomyelitis in his first right toe and fifth left toe, respectively, and amputations were performed. Meanwhile, he began to experience hearing loss, and a hearing aid was used in the right ear. After his gait became unsteady he was referred to a department of neurology. Physical examination revealed foot ulcers and mutilations (Fig. 1B). His muscle strength was normal; however, a marked decrease was observed in his sense of pain and touch (1/10) in the lower limbs. Vibration perception was present in the fingers but absent in the lower limbs, and Romberg test was positive. Mild mental retardation was noted. Examination of the cranial nerves was normal except for bilateral hearing loss. Cerebellar function examination showed no abnormalities on finger-to-nose or heel-to-knee testing, or rapidly alternating pronation and supination of hands. Muscle tone was normal, without speech abnormality. The deep tendon reflexes of the lower limbs were absent. The pure tone audiometry test suggested moderate to severe bilateral sensorineural hearing loss. A 24-h Holter monitor indicated sinus bradycardia (43/min on average). Plain radiographs showed an amputation stump of the right hallux and left little toe, accompanied by bone destruction, cortical bone thickness or sclerosis, and an irregular articular surface (Figs. 1C and 1D). Brain magnetic resonance imaging (MRI) revealed mild diffuse cerebral and cerebellar atrophy (Fig. 1E). Clinical and radiological examinations revealed several saprodontia, bronchiectasis in the middle and lower lobe of the right lung, and accessory sinusitis.

In the electrophysiological study, except for the slight slowing of motor nerve conduction velocity in the right tibial nerve, motor nerve conduction studies were almost normal in the median, ulnar, and posterior tibial nerves. However, the sensory nerve action potential could not be evoked in the right median, ulnar, and sural nerves.

The protocol of the studies described below was reviewed and approved by the Institutional Review Board of Kagoshima University. The patient provided his written informed consent to participate in this study.

Methods and Results

Sixteen candidate genes, including 11 genes related to hereditary sensory and autonomic neuropathies (HSAN) and another 5 genes (Table 1) associated with sensory and autonomic dysfunctions were screened on the MiSeq sequencing system Illumina, San Diego, CA, USA).

After one run for 28 h, 400,122 (150 × 2) reads were generated for this patient on the NGS; 93.7% of the reads could be mapped to the reference genome and 98.1% of the target regions were covered at least 10 times. In 27 high-confidence variants, 24 known single nucleotide polymorphisms (SNPs) were coincident with the dbSNP (http://www.ncbi.nlm.nih.gov/snp/) or 1000 Genomes data (http://browser.1000genomes.org). Of the remaining three non-synonymous variants, c.3248A>C in *KIF1A* and c.3448T>C in *SCN9A* were also found in the normal control, and were thus considered SNPs. Besides, a heterozygous missense mutation, c.1706A>G (p.His569Arg) in exon 21 of the *DNMT1* gene (NM_001130823.1, NP_001124295.1) remained and was confirmed by Sanger sequencing (Figs. 2A and 2B). This mutation is located in a highly conserved domain among different species (Fig. 2C). Using the web-based programs, this His569Arg alteration was predicted to be pathogenic in POLYPHEN2 (0.982) and SIFT (0.00).

This mutation was not observed in 100 Japanese control samples, nor did we find it on the 1000 Genomes web site, which catalogs human genetic variations using 2,500 samples, including 500 East Asian (100 Japanese) samples.

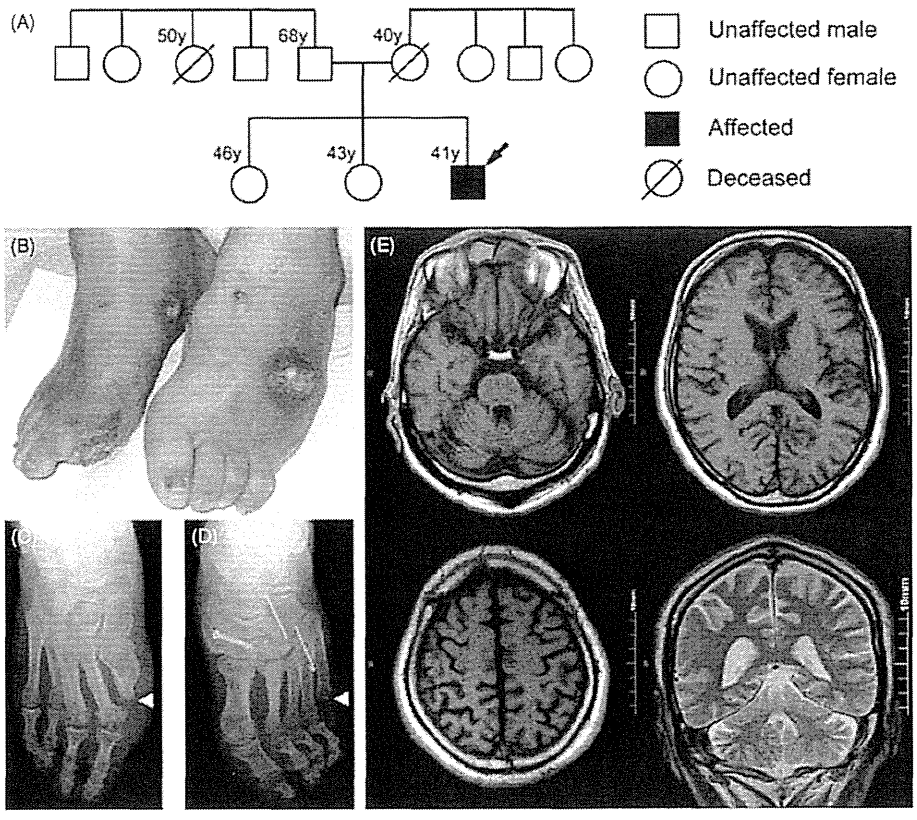

Figure 1. Pedigree and clinical photographs. (A) Pedigree of the patient. The arrow (→) indicates the index case. (B) Foot ulcers and mutilations. (C, D) Radiographs showing the amputation stump of the right hallux and left little toe (▫) accompanied by chronic osteomyelitis. (E) Brain magnetic resonance imaging showing mild and diffuse cerebral and cerebellar atrophy.

Table 1. Candidate genes screened using Miseq sequencing system.

Gene symbol	Locus	Coding exons	Reference sequences
SPTLC1	9q22.31	15	ENST00000262554
SPTLC2	14q24.3	12	ENST00000216484
ATL1	14q11	14	ENST00000441560
DNMT1	19p13.2	41	ENST00000359526
WNK1	12p13.33	28	ENST00000537687
FAM134B	5p15.1	9	ENST00000306320
KIF1A	2q37.3	49	ENST00000498729
IKBKAP	9q31.3	37	ENST00000374647
NTRK1	1q23.1	16	ENST00000368196
NGF	1p13.2	3	ENST00000369512
DST	6p12.1	84	ENST00000244364
SCN9A	2q24.3	27	ENST00000303354
CCT5	5p15.2	11	ENST00000280326
PRNP	20p13	2	ENST00000379440
FLVCR1	1q32.3	10	ENST00000366971
RNF170	8p11.21	7	ENST00000527424

Discussion

We report a Japanese patient with suspected HSAN. Using a high-throughput NGS system, we established a diagnostic procedure involving screening of 16 candidate genes in one run, and identified a novel missense mutation in exon 21 of *DNMT1*.

In 2011, *DNMT1*-related dementia, deafness, and sensory neuropathy was demonstrated in four kindreds from America, Europe, and Japan and was designated HSAN IE. It is an autosomal dominant degenerative disorder of the central and peripheral nervous systems characterized by sensory impairment, sudomotor dysfunction (loss of sweating), dementia, and sensorineural hearing loss. Affected individuals are normal in their youth but begin to manifest progressive sensorineural deafness and sensory neuropathy by the age of 20–35 *(Klein et al., 2011)*. In 2012, another four kindreds from Europe were found to have early onset (18–44 years) of a narcolepsy/cataplexy syndrome followed by ataxia, deafness, sensory neuropathy, and memory loss, which was reported to be associated with *DNMT1* mutations *(Winkelmann et al., 2012)*.

The present patient was normal until graduation from senior high school, but began to manifest progressive inability to perceive pain and experienced painless osteomyelitis. Deafness, as the second symptom, started after the age of 30, and an examination

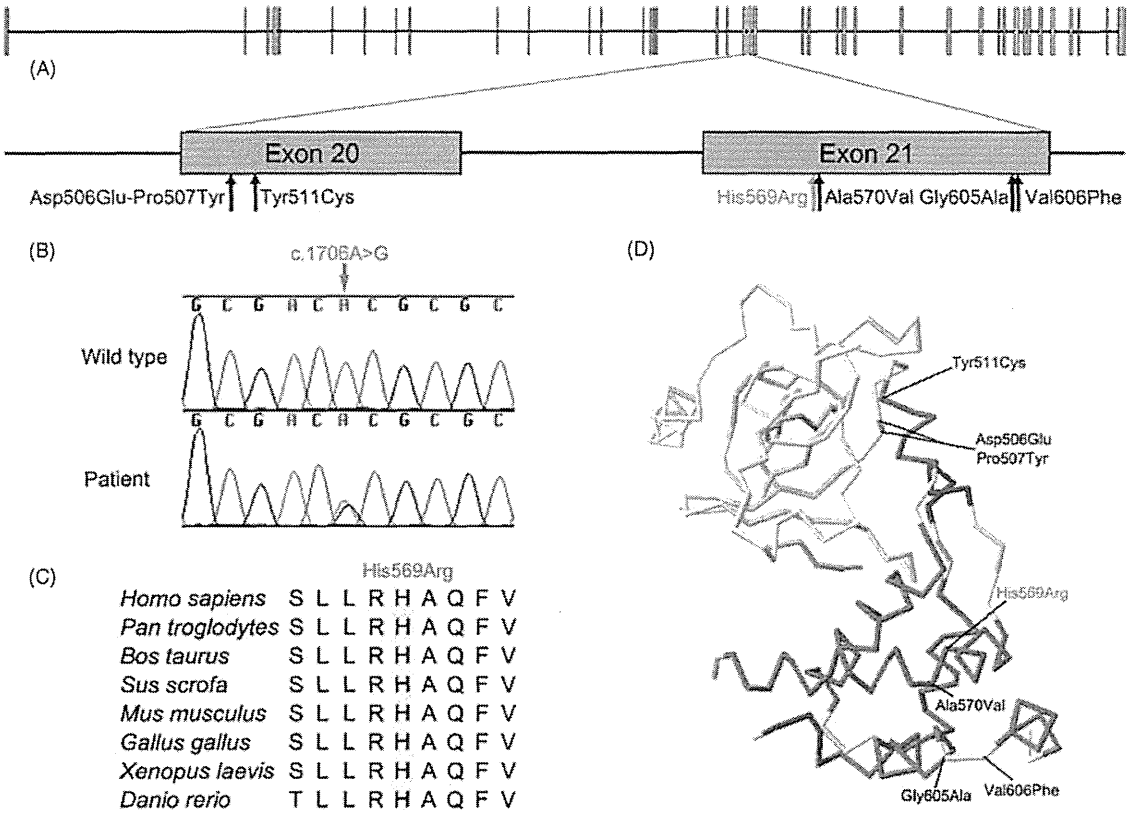

Figure 2. Genetic studies and mutations review. (A) Schematic overview and all mutations in exons 20 and 21 of *DNMT1*. (B) Sequencing chromatogram of the c.1706A>G mutation. Red arrow indicates the mutation site in present patient. (C) Amino acid sequence at the mutation site in homologs of DNA methyltransferase 1 aligned by CLUSTALW. A yellow bar indicates the highly conserved histidine at position 569. (D) Location of mutated residues in the crystal structure of the replication focus targeting sequence domain (Protein Data Bank accession number 3EPZ, showing residues 367–616 in NP_001124295.1).

revealed bilateral sensorineural hearing loss. His gait became ataxic and there was no vibration perception in the lower limbs. Although cerebellar atrophy was revealed by the brain MRI, no definite cerebellar dysfunction was identified. After examination, his ataxia was considered mainly due to loss of deep sensation. The electrophysiological studies revealed sensory dominant axonal polyneuropathy. In addition, mental retardation was observed by the neurologist and diffuse cerebral and cerebellar atrophy was noted in the brain MRI. All these findings were consistent with HSAN IE. The patient's sinus bradycardia and other dysfunctions of the respiratory system might have resulted from the autonomic nervous system dysfunction, but no reliable test was performed to check his autonomic nervous function.

Using the MiSeq sequencing system, a heterozygous missense mutation, c.1706A>G (p.His569Arg), was identified in exon 21 of *DNMT1*. As the present patient showed a definite HSAN phenotype, our findings indicated that the variable *DNMT1*-related phenotype was unlikely to have been determined by the location of the mutation. Although no narcolepsy/cataplexy was noted either in our case or the original four kindreds, the mechanism underlying the varied phenotypes requires further investigation.

It is noteworthy that all reported mutations of *DNMT1* were located in exon 20 (*Klein et al., 2011*: p.Asp506Glu-Pro507Tyr, p.Tyr511Cys; NP_001124295.1) and exon 21 (*Winkelmann et al., 2012*: p.Ala570Val, p.Gly605Ala, p.Val606Phe; NP_001124295.1), and that the original presentations were sensory neuropathy and narcolepsy/cataplexy syndrome, respectively. In Dnmt1, all the peptides encoded by exons 20 and 21 belong to the RFTS domain (Fig. 2D). Previous research indicated that this RFTS domain, inserted deeply into the DNA-binding pocket *(Takeshita et al., 2011)*, contributes to the inhibition of Dnmt1 binding to naked DNA oligonucleotides and native polynucleosomes *(Syeda et al., 2011)*. The RFTS domain also contains a binding site for Uhrf1 *(Achour et al., 2008)*, which recognizes and binds to the hemimethylation sites of DNA and recruits Dnmt1 *(Bostick et al., 2007; Arita et al., 2008;*

Avvakumov et al., 2008). Mutations in exon 20 and 21 of *DNMT1* would transform the structure of the RFTS domain and affect the recognition and binding procedure of hemimethylated DNA, creating abnormal methylation and gene silencing. On the basis of our findings and previous studies, we surmise that the RFTS domain is a mutation hot spot compared with the other Dnmt1 domains. The other possibility is that mutation in other functional domains might cause global genome demethylation and embryonic lethality.

In conclusion, using a MiSeq sequencing system we identified a novel missense mutation in exon 21 of *DNMT1* in a Japanese patient with the typical HSAN IE phenotype. We also reviewed all eight of the kindreds with *DNMT1* mutations in previous reports, and excluded the presumption that varied phenotypes were generated by mutations in different exons. However, further research is required to elucidate the mechanisms of alterations in the RFTS domain and their influence on the DNA methylation procedure.

Acknowledgements

The authors thank Ms. A. Nishibeppu of our department for her excellent technical assistance. The authors would like to thank Enago (www.enago.jp) for the English language review. The authors thank the Joint Research Laboratory, Kagoshima University Graduate School of Medical and Dental Sciences for the use of their facilities. The study was funded by the research on the Nervous and Mental Disorders and Research Committee for Charcot-Marie-Tooth Disease, Neuropathy, Ataxic Disease and Applying Health and Technology of Ministry of Health, Welfare and Labour, Japan.

References

Achour M, Jacq X, Rondé P, Alhosin M, Charlot C, Chataigneau T, Jeanblanc M, Macaluso M, Giordano A, Hughes AD, Schini-Kerth VB, Bronner C (2008). The interaction of the SRA domain of ICBP90 with a novel domain of DNMT1 is involved in the regulation of VEGF gene expression. Oncogene 27:2187–2197.

Arita K, Ariyoshi M, Tochio H, Nakamura Y, Shirakawa M (2008). Recognition of hemi-methylated DNA by the SRA protein UHRF1 by a base-flipping mechanism. Nature 455:818–821.

Avvakumov GV, Walker JR, Xue S, Li Y, Duan S, Bronner C, Arrowsmith CH, Dhe-Paganon S (2008). Structural basis for recognition of hemi-methylated DNA by the SRA domain of human UHRF1. Nature 455:822–825.

Bostick M, Kim JK, Estève PO, Clark A, Pradhan S, Jacobsen SE (2007). UHRF1 plays a role in maintaining DNA methylation in mammalian cells. Science 317:1760–1764.

Chen WG, Chang Q, Lin Y, Meissner A, West AE, Griffith EC, Jaenisch R, Greenberg ME (2003). Derepression of BDNF transcription involves calcium-dependent phosphorylation of MeCP2. Science 302:885–889.

Feng J, Fan G (2009). The role of DNA methylation in the central nervous system and neuropsychiatric disorders. Int Rev Neurobiol 89:67–84.

Klein CJ, Botuyan MV, Wu Y, Ward CJ, Nicholson GA, Hammans S, Hojo K, Yamanishi H, Karpf AR, Wallace DC, Simon M, Lander C, Boardman LA, Cunningham JM, Smith GE, Litchy WJ, Boes B, Atkinson EJ, Middha SB, Dyck PJ, Parisi JE, Mer G, Smith DI, Dyck PJ (2011). Mutations in DNMT1 cause hereditary sensory neuropathy with dementia and hearing loss. Nat Genet 43:595–600.

Syeda F, Fagan RL, Wean M, Avvakumov GV, Walker JR, Xue S, Dhe-Paganon S, Brenner C (2011). The replication focus targeting sequence (RFTS) domain is a DNA-competitive inhibitor of Dnmt1. J Biol Chem 286:15344–15351.

Takeshita K, Suetake I, Yamashita E, Suga M, Narita H, Nakagawa A, Tajima S (2011). Structural insight into maintenance methylation by mouse DNA methyltransferase 1 (Dnmt1). Proc Natl Acad Sci U S A 108:9055–9059.

Tohgi H, Utsugisawa K, Nagane Y, Yoshimura M, Genda Y, Ukitsu M (1999). Reduction with age in methylcytosine in the promoter region −224 approximately −101 of the amyloid precursor protein gene in autopsy human cortex. Brain Res Mol Brain Res 70:288–292.

Winkelmann J, Lin L, Schormair B, Kornum BR, Faraco J, Plazzi G, Melberg A, Cornelio F, Urban AE, Pizza F, Poli F, Grubert F, Wieland T, Graf E, Hallmayer J, Strom TM, Mignot E (2012). Mutations in DNMT1 cause autosomal dominant cerebellar ataxia, deafness and narcolepsy. Hum Mol Genet 21:2205–2210.

Pediatric Neurology 48 (2013) 59–62

Contents lists available at ScienceDirect

Pediatric Neurology

journal homepage: www.elsevier.com/locate/pnu

Case Report

Congenital Hypomyelinating Neuropathy Attributable to a De Novo p.Asp61Asn Mutation of the Myelin Protein Zero Gene

Takahiro Yonekawa MD [a], Hirofumi Komaki MD, PhD [a,*], Yuko Saito MD, PhD [b], Hiroshi Takashima MD, PhD [c], Masayuki Sasaki MD, PhD [a]

[a] *Department of Child Neurology, National Center of Neurology and Psychiatry, National Center Hospital, Tokyo, Japan*
[b] *Department of Pathology and Laboratory Medicine, National Center of Neurology and Psychiatry, National Center Hospital, Tokyo, Japan*
[c] *Department of Neurology and Geriatrics, Graduate School of Medical and Dental Sciences, Kagoshima University, Kagoshima, Japan*

ARTICLE INFORMATION

Article history:
Received 31 July 2012
Accepted 13 September 2012

ABSTRACT

We describe a boy aged 2 years and 11 months with congenital hypomyelinating neuropathy attributable to a de novo heterozygous missense mutation of c.181G>A (p.Asp61Asn) in the myelin protein zero gene. A nerve conduction study indicated markedly reduced motor conduction velocities in the upper and lower extremities. Stimuli of up to 50-100 mA were necessary for nerve activation, suggesting diseased nerves with greatly decreased excitability. A sural nerve biopsy revealed a marked loss of large myelinated fibers, the absence of myelin breakdown products, occasional basal lamina onion-bulb formations, and tomacula-like structures. The p.Asp61Asn mutation is novel in congenital hypomyelinating neuropathy, but was previously reported in a patient with Charcot-Marie-Tooth disease type 1.

Introduction

Congenital hypomyelinating neuropathy constitutes a rare congenital neuropathy characterized by onset prenatally, neonatally, or during early infancy, with hypotonia, nonprogressive weakness, markedly reduced nerve conduction velocities, and hypomyelination. Molecular genetic analyses revealed that several mutations in five genes encoding proteins involved in peripheral nerve myelination (i.e., *MPZ*, *PMP22*, *ERG2*, *MTMR2*, and *SOX10*) can cause congenital hypomyelinating neuropathy [1].

Myelin protein zero is a transmembrane protein of the immunoglobulin family and an important myelin structural protein required for normal peripheral nerve myelination. More than 120 mutations in the *MPZ* gene have been detected in patients with various forms of hereditary motor and sensory neuropathies [1]. Recent clinical and laboratory investigations provided insights into the pathogenesis of neuropathies associated with these *MPZ* mutations. Myelin protein zero contains a large glycosylated immunoglobulin-like extracellular domain that endows proteins with adhesion properties, and a smaller basic intracellular domain that participates in electrostatic interactions [2]. To our knowledge, eight mutations (i.e., p.Arg98Cys, p.Ser111Phe, p.Gly123_Cys127del, p.Thr124Lys, p.Asn131Ser, p.Gly167Arg, p.Leu184fs, and p.Gln215X) in the *MPZ* gene have been demonstrated to segregate with congenital hypomyelinating neuropathy [1,3-5]. Among these, five and two mutations were identified in the extracellular and intracellular domains, respectively, of *MPZ* gene products.

We report on a Japanese boy with congenital hypomyelinating neuropathy attributable to a de novo heterozygous mutation of c.181G>A (p.Asp61Asn) in the *MPZ* gene. This patient presented with clinical, electrophysiologic, and morphologic features consistent with congenital hypomyelinating neuropathy.

Case Report

A boy aged 2 years and 11 months was evaluated for gross motor delay and generalized hypotonia. No family history of neuromuscular disease was reported. The parents were not consanguineous. The patient's older brother was healthy and developmentally normal. The pregnancy was reportedly normal, with no history of decreased fetal

* Communications should be addressed to: Dr. Komaki; Department of Child Neurology; National Center of Neurology and Psychiatry; National Center Hospital; 4-1-1 Ogawa-Higashicho; Kodaira, Tokyo 187 8551, Japan.
E-mail address: komakih@ncnp.go.jp

0887-8994/$ - see front matter © 2013 Elsevier Inc. All rights reserved.
http://dx.doi.org/10.1016/j.pediatrneurol.2012.09.011

movements. The patient was delivered uneventfully at 37 weeks of gestation. His birth weight was 2884 g. He sat independently at age 8 months, but was unable to stand with support at 12 months of age. He began crawling at age 15 months, and walked independently at age 2 years and 3 months. He was unable to run. His language development and fine motor development were normal.

He was alert and bright, but his face appeared myopathic. Physical examination revealed a mildly high-arched palate, but neither thenar plus hypothenar atrophy nor pes cavus. A cranial nerve examination revealed normal ocular movements and pupillary responses to light. Mild facial muscle weakness was evident. Tongue fasciculations were absent. He was hypotonic, but his muscle strength was only mildly reduced in the four extremities. Hyperextension was observed in the finger, wrist, and knee joints. His muscle bulk was normal. Deep tendon reflexes were absent at the biceps, triceps, patella, and ankles. No sensory disturbance was evident. The Romberg sign was demonstrated as negative. Truncal titubation and dysmetria were absent. He was able to stand up from a supine position using a modified Gowers maneuver. His gait, with bilateral genu recurvatum, was wide-based and ataxic.

His creatine kinase level was measured at 166 IU/L (normal range, 62-287 IU/L). Cerebrospinal fluid testing demonstrated mildly elevated protein content (54 mg/dL; normal range, 10-40 mg/dL) and a few mononuclear cells. Cranial magnetic resonance imaging indicated no intracranial abnormalities. A nerve conduction study revealed very prolonged distal latencies, markedly reduced motor conduction velocities (3.0-4.0 m/second), and the temporal dispersion of compound muscle action potentials from his upper and lower extremities (data not shown). To evoke motor nerve responses, electrical stimuli greater than 50 mA were necessary. Sensory responses were not evoked (data not shown). Magnetic resonance imaging of the lumbar plexus demonstrated no enlarged nerve roots. A sural nerve biopsy revealed a severe loss of large myelinated fibers in all fascicles. Well-organized onion-bulb formations were not evident (Fig 1a). No inflammatory infiltrates, edema, or storage materials were observed. Intramuscular nerves rarely included large myelinated fibers (data not shown). A teased fiber analysis demonstrated thin, myelinated segments and tomacula-like structures (Fig 1b). Electron microscopic examination revealed occasional onion-bulb formations consisting of multilayered empty basal lamina (Fig 1c). Occasional fibers with thin or abnormally compacted myelin (Fig 1d) were also observed. Unmyelinated fibers were well preserved. A peroneus brevis muscle biopsy indicated mild variations in fiber size, without necrotic or regenerating fibers. We detected no evidence of group atrophy. Each fiber type was distributed in a mosaic pattern, without evidence of fiber type grouping. However, type 1 fibers were mildly atrophic (data not shown). Gene resequencing according to the DNA chip technique revealed one allele to possess a de novo point mutation, c.181G>A (p.Asp61Asn), in the extracellular domain of *MPZ*. A purpose-built GeneChip CustomSeq Custom Resequencing Array (Affymetrix, Santa Clara, CA) was designed to screen for mutations of 28 disease-causing genes in Charcot-Marie-Tooth disease, congenital hypomyelinating neuropathy, and related diseases such as ataxia with oculomotor apraxia type 1, ataxia with oculomotor apraxia type 2, spinocerebellar ataxia with axonal neuropathy type 1, and hereditary motor neuropathies [6]. The p.Asp61Asn mutation was confirmed by the conventional Sanger DNA sequencing method. The patient's healthy parents and brother did not manifest this mutation.

Discussion

Inherited neuropathy with hypomyelination remains controversial nosologically, and congenital hypomyelinating neuropathy can be difficult to differentiate from the early-onset form of hereditary motor and sensory neuropathy

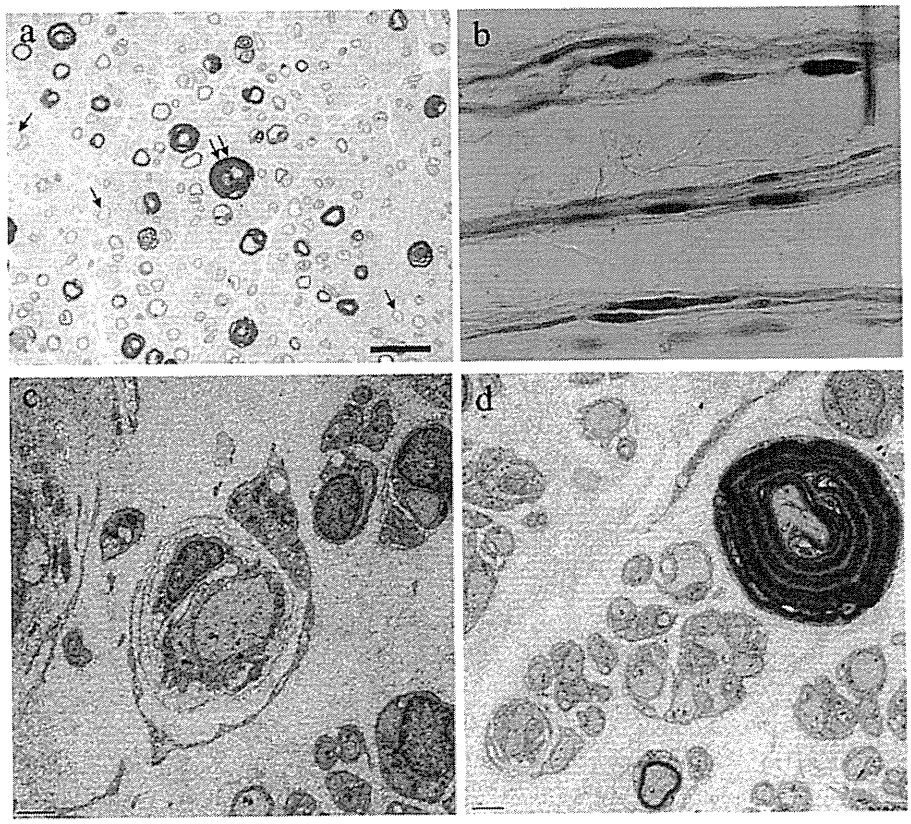

Figure 1. (a) Epoxy-embedded and toluidine blue-stained semithin section of the sural nerve reveals the endoneurium, including nonmyelinated (arrows), hypomyelinated, and hypermyelinated (double arrows) fibers. Bar, 20 μm. (b) Teased fiber analysis demonstrates thin, myelinated segments and tomacula-like structures. A lack of myelination is evident in the nerves. (c) Electron microscopy reveals an absence of myelin and onion-bulb formations consisting of multilayered empty basal lamina. Bar, 2 μm. (d) Electron microscopy indicates abnormally compacted myelin. Bar, 2 μm.

type 3 (Déjérine-Sottas syndrome) on a clinical basis alone. These phenotypes, it has been argued, are distinct entities with unique clinical and morphologic features, e.g., congenital hypomyelinating neuropathy is a disorder of myelin formation, whereas Déjérine-Sottas syndrome is a demyelinating disorder. On the other hand, they may occur within a continuum of "myelinopathies," differing in severity but with a common underlying defect in myelination [2]. Because repeated demyelination and remyelination are known to be responsible for the onion-bulb formation in Charcot-Marie-Tooth disease or the Déjérine-Sottas syndrome of hereditary motor and sensory neuropathies, nerve pathology can assist in differentiating between congenital hypomyelinating neuropathy and Déjérine-Sottas syndrome in the absence of myelin breakdown, well-organized onion-bulb formation, and inflammation in congenital hypomyelinating neuropathy [7].

Our patient was a young boy with sensorimotor congenital neuropathy presenting as gross motor delay, nonprogressive weakness, and hypotonia. Histopathologic images of the sural nerve were compatible with congenital hypomyelinating neuropathy. According to a nerve conduction study, stimuli as strong as 50-100 mA were necessary for nerve activation, indicating diseased nerves with markedly decreased excitability [8]. No evidence of myelin breakdown products was detected, indicating that little, if any, demyelination and remyelination were occurring. According to muscle pathology, group atrophy was absent, and the mosaic pattern of each fiber type was well-preserved. These findings suggest that the axons were most likely intact during muscle fiber growth and fiber type differentiation. In contrast with patients manifesting Déjérine-Sottas syndrome, our patient presented no evidence of repeated demyelination, but did demonstrate occasional, atypical onion-bulb formations consisting of multilayered empty basal lamina. Mild type 1 fiber atrophy was present in our patient.

Interestingly, previous reports demonstrated that muscle pathology in congenital hypomyelinating neuropathy included type 2 fiber atrophy with type 1 fiber predominance and type 1 fiber hypotrophy and predominance [4,7], although the pathogenesis underlying type 1 fiber atrophy in our patient remains unknown.

The p.Asp61Asn mutation in the *MPZ* gene was reported by Bellone et al. to be a pathogenic mutation in a patient with Charcot-Marie-Tooth disease type 1 [9,10]. This mutation is also responsible for congenital hypomyelinating neuropathy. Similarly, the p.Gly167Arg mutation was reported to contribute to congenital hypomyelinating neuropathy, Déjérine-Sottas syndrome, and Charcot-Marie-Tooth disease type 1 [1]. More than 120 mutations in the *MPZ* gene (most of which are localized within the extracellular domain of the protein) are known to cause various hereditary motor and sensory neuropathies [1]. The *MPZ* gene encodes a transmembrane protein of 219 amino acids, and contains a single extracellular domain, a single transmembrane domain, and a single cytoplasmic domain [11]. Crystallographic analysis of the *MPZ* extracellular domain demonstrates that it forms homotetramers within the plane of the membrane, and that each of them interacts with a similar homotetramer on the opposing membrane surface [12]. Furthermore, the absence of *MPZ* expression in animals, such as *Mpz* knockout mice, causes myelin to lose its normal compact state [13]. According to these data, myelin protein zero plays an essential role in the myelination of the peripheral nervous system, probably by holding together adjacent wraps of the myelin membrane via homotypic interactions mediated by myelin protein zero. Distinct phenotypes associated with different mutations at the same position may be attributable to a primary role played by amino acid changes [14]. However, the pathogenic mechanisms by which a single mutation in the *MPZ* gene can cause two hereditary motor and sensory neuropathic phenotypes remain unknown. Molecular modeling indicates that the substitution of p.Asp61Asn produces a variation in polarity, consequently affects the network of hydrogen bonds responsible for the correct folding and dimerization of the protein, and is associated with severe early-onset demyelinating neuropathy [10]. The presence of the p.Asp61Asn heterozygous mutation in our patient suggests that a mutated allele of the *MPZ* gene exerts a dominant-negative effect. Further functional studies are required to understand the pathogenic impacts of the p.Asp61Asn mutation on clinical phenotypes.

The authors thank Ichizo Nishino, MD, PhD, for the critical evaluation of muscle pathology, Yasushi Oya, MD, PhD, for helpful discussions, Yoriko Kojima for technical support with electron microscopic studies, and Akiko Yoshimura, BS, of Kagoshima University for excellent technical assistance. This work was supported by a Grant-in-Aid from the Research Committee of Spinal Muscular Atrophy at the Ministry of Health, Labor, and Welfare of Japan, and by Intramural Research Grant 23-6 for Neurologic and Psychiatric Disorders of the National Center of Neurology and Psychiatry (to T.Y. and H.K.). This study was also supported in part by grants from the Nervous and Mental Disorders and Research Committee for Charcot-Marie-Tooth Disease, Neuropathy, Ataxic Disease, and Research on Applying Health Technology at the Japanese Ministry of Health, Welfare and Labor (to H.T.).

Supplementary material

Supplementary material associated with this article is available, in the online version, at doi:10.1016/j.pediatrneurol.2012.09.011.

References

[1] Inherited Peripheral Neuropathies Mutation Database (IPNMDB). Available at: http://www.molgen.ua.ac.be/CMTMutations/. Accessed April 3, 2012.
[2] Warner LE, Hilz MJ, Appel SH, et al. Clinical phenotypes of different *MPZ* (P0) mutations may include Charcot-Marie-Tooth type 1B, Déjérine-Sottas, and congenital hypomyelination. Neuron 1996; 17:451–60.
[3] Phillips JP, Warner LE, Lupski JR, Garg BP. Congenital hypomyelinating neuropathy: Two patients with long-term follow-up. Pediatr Neurol 1999;20:226–32.
[4] Sevilla T, Lupo V, Sivera R, et al. Congenital hypomyelinating neuropathy due to a novel *MPZ* mutation. J Peripher Nerv Syst 2011;16:347–52.
[5] McMillan HJ, Santagata S, Shapiro F, et al. Novel mutations and congenital hypomyelinating neuropathy. Neuromuscul Disord 2010;20:725–9.
[6] Nakamura T, Hashiguchi A, Suzuki S, Uozumi K, Tokunaga S, Takashima H. Vincristine exacerbates asymptomatic Charcot-Marie-Tooth disease with a novel *ERG2* mutation. Neurogenetics 2012;13:77–82.
[7] Nara T, Akashi M, Nonaka I, et al. Muscle and intramuscular nerve pathology in congenital hypomyelination neuropathy. J Neurol Sci 1995;129:170–4.

[8] Kimura J. Nerve conduction and needle electromyography. In: Dick PJ, Thomas PK, editors. Peripheral neuropathy. 4th ed. Philadelphia: Elsevier Saunders; 2005. p. 900.
[9] Bellone E, Cassandrini D, Di Maria E, et al. Novel *MPZ* mutation in a sporadic CMT patient [abstract]. J Periph Nerv Syst 2001;6:41.
[10] Mandich P, Fossa P, Capponi S, et al. Clinical features and molecular modeling of novel *MPZ* mutations in demyelinating and axonal neuropathies. Eur J Hum Genet 2009;17:1129–34.
[11] Lemke G, Axel R. Isolation and sequence of a cDNA encoding the major structural protein of peripheral myelin. Cell 1985;40:501–8.
[12] Shapiro L, Doyle JP, Hensley P, Colman DR, Hendrickson WA. Crystal structure of the extracellular domain from P0, the major structural protein of peripheral nerve myelin. Neuron 1996;17: 435–49.
[13] Giese KP, Martini R, Lemke G, Soriano P, Schachner M. Mouse P0 gene disruption leads to hypomyelination, abnormal expression of recognition molecules, and degeneration of myelin and axons. Cell 1992;71:565–76.
[14] Shy ME, Jáni A, Krajewski K, et al. Phenotypic clustering in *MPZ* mutations. Brain 2004;127:371–84.

DIABETES RESEARCH AND CLINICAL PRACTICE XXX (2012) XXX–XXX

Contents available at Sciverse ScienceDirect

Diabetes Research and Clinical Practice

journal homepage: www.elsevier.com/locate/diabres

International Diabetes Federation

Intraepidermal nerve fiber density and nerve conduction study parameters correlate with clinical staging of diabetic polyneuropathy

Aiko Arimura [a,b], *Takahisa Deguchi* [a,b,*], *Kazuhiro Sugimoto* [c], *Tadashi Uto* [a], *Tomonori Nakamura* [a], *Yumiko Arimura* [a], *Kimiyoshi Arimura* [d], *Soroku Yagihashi* [e], *Yoshihiko Nishio* [b], *Hiroshi Takashima* [a]

[a] *Department of Neurology and Geriatrics, Kagoshima University Graduate School of Medical and Dental Sciences, Kagoshima, Japan*
[b] *Department of Diabetes and Endocrine Medicine, Hematology, Endocrinology and Diabetology Center, Kagoshima University Hospital, Kagoshima, Japan*
[c] *Diabetes Center, Ohta Nishinouchi Hospital, Fukushima, Japan*
[d] *Ohkatsu Neurology and Rehabilitation Hospital, Kagoshima, Japan*
[e] *Department of Pathology and Molecular Medicine, Hirosaki University Graduate School of Medicine, Hirosaki, Japan*

ARTICLE INFO

Article history:
Received 8 February 2012
Received in revised form
9 June 2012
Accepted 4 September 2012

Keywords:
Clinical staging of diabetic polyneuropathy
Intraepidermal nerve fiber densities
Nerve conduction studies

ABSTRACT

Aim and methods: To assess the usefulness of the diagnostic and staging criteria for diabetic polyneuropathy (DP) by the Diabetic Neuropathy Study Group in Japan (DNSGJ) we examined clinical features, intraepidermal nerve fiber densities (IENFD) and nerve conduction studies (NCS) and coefficient of variation of the R-R intervals (CVR-R) in 44 patients with diabetes. *Results:* The patients were classified into stage I ($n = 20$), II ($n = 6$), III + IV ($n = 12$), and V ($n = 6$) according to the staging criteria by DNSGJ. IENFD decreased as stages progressed (13.8 ± 7.1 fiber/mm in stage I to 0.8 ± 1.3 fiber/mm in stage V). Compound motor and sensory action potential and motor and sensory nerve conduction velocity decreased with progressing stage. F-wave latency prolonged as stages progressed. CVR-R decreased with progressing stage ($4.41\% \pm 2.65\%$ in stage I to $1.33\% \pm 0.57\%$ in stage V). IENFD correlated with the various parameters of NCS ($r = 0.378$–0.636, $p < 0.05$) and CVR-R ($r = 0.399$, $p = 0.007$). *Conclusions:* Clinical staging for DP by DNSGJ reflects the results of small and large fiber neuropathy.

1. Introduction

Diabetic neuropathy considered a mixed neuropathy of both large- and small-fiber types develops gradually and symmetrically. The symptoms, such as numbness, tingling, pins and needles, and tightness in the feet suggest the involvement of thick myelinated Aβ fibers. Burning or a cold sensation and pain of various types with autonomic symptoms suggest the damage of thinly myelinated Aγ and unmyelinated C fibers ("small fiber neuropathy") [1].

Neurological signs are also classified into small-fiber signs (impaired sensations to a pinprick, heat, and cold) and large-fiber signs (impaired vibratory and joint sense) [2,3]. In addition, nerve conduction studies (NCSs) are performed as a clinical assessment to evaluate large-fiber neuropathy, and

* *Corresponding author at:* Department of Neurology and Geriatrics, Kagoshima University Graduate School of Medical and Dental Sciences, 8-35-1 Sakuragaoka, Kagoshima 890-8520, Japan. Tel.: +81 99 275 5332; fax: +81 99 265 7164.
E-mail address: degdeg@m3.kufm.kagoshima-u.ac.jp (T. Deguchi).
0168-8227/$ – see front matter © 2012 Elsevier Ireland Ltd. All rights reserved.
http://dx.doi.org/10.1016/j.diabres.2012.09.026

Please cite this article in press as: Arimura A, et al. Intraepidermal nerve fiber density and nerve conduction study parameters correlate with clinical staging of diabetic polyneuropathy. Diabetes Res Clin Pract (2012), http://dx.doi.org/10.1016/j.diabres.2012.09.026

skin innervation is useful as a parameter of small-fiber sensory neuropathy [4,5].

Several criteria and staging systems of diabetic polyneuropathy (DP) have been introduced [6,7]. Dyck et al. reported DP diagnostic criteria, including the presence of any abnormality (nerve conduction velocity, amplitude, or latency) in two or more nerves on an electrophysiological test [6]. The Diabetes Control and Complications Trial used neurological findings in two of these three categories (objective neuropathic symptoms, abnormal sensation, and decreased reflex) as clinical DP criteria [7]. In the longitudinal Rochester Diabetic Neuropathy Study cohort, the authors recommended using composite score criteria, including the Neuropathy Impairment Score of the lower limbs plus seven tests to stage DP severity [8]. The criteria for abnormal nerve conduction in two or more nerves showed 81% sensitivity and 91.2% specificity [8]; thus, the criteria have been frequently used as the gold standard. But these criteria are less commonly used in clinical practice, because of the difficulty to use and requirement of an NCS [6,9–11].

Consequently, the Diabetic Neuropathy Study Group in Japan (DNSGJ) proposed simplified diagnostic criteria and clinical DP staging for daily practice [12,13]. Yasuda et al. reported that sensory nerve action potential (SNAP) and sensory conduction velocity of the sural nerve decrease with progressing the stage [12]. Although the clinical staging for DP reflects large fiber neuropathy, little has been reported on small fiber neuropathy. A correlation between clinical DP staging by DNSGJ and Dyck's staging and nerve function has been reported [12]. However, previous studies did not include neurological examination of small fiber neuropathy.

In the present study, we examined patients with diabetes by determining intraepidermal nerve fiber density (IENFD), conducting NCSs, and calculating the coefficient of variation for the RR interval (CVR-R) on an electrocardiogram to evaluate small and large fiber neuropathy for the purpose of verifying the usefulness of clinical staging for DP by DNSGJ.

2. Research design and methods

2.1. Patient selection

Fourteen inpatients with diabetes mellitus and 30 outpatients were enrolled from 2008 to 2011 at the Department of Diabetes and Endocrine Medicine, Hematology, Endocrinology and Diabetology Center, and Neurology and Geriatrics Center, Kagoshima University Medical and Dental Hospital.

Body mass index (BMI), diabetes duration, and glycated hemoglobin (HbA1c) level were evaluated in all patients. The value of HbA1c was express as equivalent to the National Glycohemoglobin Standardization Program (NGSP) value defined by the Japan Diabetes Society (JDS) [14]. Subjective symptoms, including numbness, pain, dysesthesia, paresthesia, and allodynia in the tips of toes or bottoms of feet bilaterally, a clinical neurological examination (vibratory sensation on bilateral medial malleoli evaluated with a C128 Hz tuning fork, ankle reflex, sensory test by monofilament, ankle muscle weakness, or atrophy), autonomic symptoms (orthostatic hypotension, abnormal sweating, severe diarrhea, and constipation), diabetic complications and quality of life were tested and recorded [12]. We excluded patients with other peripheral neuropathies, such as Sjogren's syndrome, alcoholic neuropathy, immunoglobulin A nephropathy, and treatment-induced diabetic neuropathy.

The diagnostic criteria for DP by DNSGJ are two or more abnormalities of three neurological examination items. (1) Presence of symptom considered to be due to diabetic polyneuropathy; (2) decrease or disappearance of bilateral ankle reflex; (3) decreased vibration in bilateral medial malleoli [12]. The subjects were classified into the following staging. Stage I is no neuropathy, which does not meet the diagnostic criteria for DP by DNSGJ. Stage II is asymptomatic neuropathy in which patients do not have any subjective symptoms but meet the diagnostic criteria. At stage III, subjective symptoms are positive but either ankle reflex or vibration sense is within normal range. At stage IV, patients show clinically manifest autonomic neuropathy such as orthostatic hypotension. Motor neuropathy appears at stage V [12].

These studies were performed with the approval of the Department of Neurology and Geriatrics, Kagoshima University Graduate School of Medical and Dental sciences, and all subjects gave written informed consent.

2.2. Skin biopsy

All participants underwent a skin biopsy to determine IENFD according to the European guidelines [15]. Biopsies were taken 10 cm above the lateral malleolus. Immunofluorescence procedures were used to identify neurons in skin biopsies in a modification of the protocol described by Kennedy [16]. Tissue samples were immediately fixed in Zamboni's solution (2% paraformaldehyde, picric acid) for 12–24 h at 4 °C. Samples were subsequently cryoprotected in phosphate buffer with 20% sucrose overnight and frozen for later cryosectioning.

2.2.1. Immunofluorescence

Biopsy specimens were cut into 60 μm sections on a freezing microtome. To visualize axons and basement membranes and trace IENF from the site where the nerves penetrate the basement membrane to their endings, antibodies to PGP 9.5 (Millipore, Bedford, MA, USA, diluted 1:4000 in 1% normal serum/Tris) and type IV collagen (Chemicon, Temecula, CA, USA, diluted 1:800 in 1% normal serum/Tris) were localized by double staining using Alexa 594 (Molecular Probes, Eugene, OR, USA; diluted 1:200 in 1% normal serum/Tris) and Alexa 488 (Molecular Probes, diluted 1:200 in 1% normal serum/Tris) labeled secondary antibodies. Sections were coverslipped and mounted after washing.

2.2.2. Viewing and analysis

PGP 9.5-immunoreactive nerve fibers above the basement membrane were counted at a magnification of 40× with an Olympus Fluoview scanning laser confocal microscope (Tokyo, Japan). Eight to ten fields from at least two different sections from each specimen were collected for analysis. IENFD was quantified on images based on a stack of consecutive 2-μm optical sections (usually 16 sections) for a standard linear length of epidermis (1 mm).

Please cite this article in press as: Arimura A, et al. Intraepidermal nerve fiber density and nerve conduction study parameters correlate with clinical staging of diabetic polyneuropathy. Diabetes Res Clin Pract (2012), http://dx.doi.org/10.1016/j.diabres.2012.09.026

2.3. NCS

Nerve conduction studies were performed using conventional procedures with electromyography machines (Viking Select and Quest, Care Fusion Japan, Tokyo, Japan) following standardized methods recommended by the Consensus Development Conference on Standardized Measures in Diabetic Neuropathy (Consensus Development Conference, 1992). Skin temperature was maintained above 32 °C. SNAP amplitudes, compound muscle action potentials (CMAPs), sensory conduction velocity, motor conduction velocity of the conducting fibers, and minimal F wave latencies were recorded for analysis. Motor nerve studies were performed on the median and tibial nerves and sensory nerve were performed on the median and sural nerves.

2.4. CVR-R

All patients underwent CVR-R testing of the autonomic nervous system. CVR-R testing is a simple and reliable cardiovagal function test that detects the presence of DP with nearly the same sensitivity as a NCS [17]. CVR-R was calculated from the R-R intervals of 100 samples on electrocardiogram.

$$\text{CVR-R} = \frac{\text{SD}}{\text{average of R-R intervals}} \times 100\%$$

2.5. Statistics

Values are presented as means ± SD or as percentages for categorical data. Differences among the four groups were analyzed with a one-way analysis of variance or the Kruskal–Wallis test or Fisher's exact probability method. Post hoc group comparisons were conducted with Tukey's test or the Games–Howell test. The correlation between IENFD and diabetic parameters was refined using Spearman's rank correlation coefficient. A similar analysis was performed for CVR-R and the NCS findings. A p-value <0.05 was considered significant. All analyses were performed with SPSS version 18.0 statistical package (SPSS, Inc., Chicago, IL, USA).

3. Results

Characteristics of the patients are shown in Table 1. Among 44 patients with diabetes, 20 were classified into stage I, six into stage II, 10 into stage III, two into stage IV, and six into stage V. Because the number of patients in stage IV was limited, the data were not analyzed statistically. Yasuda reported that stages III and IV appropriated stage 2 in Dyck' s staging [12]. Thus, we combined stages III and IV, and used partially modified the staging for DP by DNSGJ. The majority of subjects had type 2 diabetes, and two patients had type 1 diabetes.

No significant difference was found among the four groups for age ($p = 0.743$), BMI ($p = 0.394$), HbA1c ($p = 0.512$), or duration of diabetes ($p = 0.338$). The percentage of diabetic retinopathy and diabetic nephropathy increased appreciably with stage. The percentage of patients with DP neuropathic symptoms were 10.0% in stage I, 16.7% in stage II, 100% in stage III + IV, and 100% in stage V ($p < 0.001$). The percentage of patients with pain as a symptom of small fiber neuropathy were 0% in stage I, 0% in stage II, 33.3% in stage III + IV, and 33.3% in stage V ($p = 0.014$). The percentage of abnormal nerve conduction in two or more nerves were 35.0% in stage I, 100%

Table 1 – The characteristic of diabetic patients in diabetic polyneuropathy staging.

	Stage I	Stage II	Stage III + IV	Stage V	p values
N (female)	20 (3)	6 (6)	12 (5)	6 (0)	
Age (years)	54.7 ± 11.3	60.2 ± 6.0	55.3 ± 14.4	51.8 ± 11.6	0.743
BMI (kg/m^2)	24.6 ± 4.6	24.7 ± 2.6	25.5 ± 7.3	23.1 ± 9.7	0.394
HbA1c (JDS, %)	7.3 ± 1.8	7.2 ± 1.1	8.2 ± 3.0	10.1 ± 3.9	0.512
Duration of diabetes (year)	10.6 ± 7.4	14.7 ± 4.6	10.9 ± 8.0	16.2 ± 12.0	0.338
Insulin treatment, n (%)	6 (30.0%)	5 (83.3%)	8 (66.7%)	6 (100%)	0.001
Retinopathy					0.014
NDR, n (%)	16 (80.0%)	1 (16.7%)	4 (33.3%)	1 (16.7%)	
SDR, n (%)	1 (5.0%)	2 (33.3%)	2 (16.7%)	3 (50%)	
PPDR, n (%)	0 (0%)	0 (0%)	2 (16.7%)	1 (16.7%)	
PDR, n (%)	3 (15.0%)	3 (50.0%)	4 (33.3%)	1 (16.7%)	
Nephropathy					0.001
Normoalbuminuria, n (%)	14 (70.0%)	5 (83.3%)	2 (16.7%)	0 (0%)	
Microalbuminuria, n (%)	1 (5.0%)	0 (0%)	5 (41.7%)	2 (33.3%)	
Overt proteinuria, n (%)	5 (25.0%)	1 (16.7%)	5 (41.7%)	4 (66.7%)	
Neuropathy					
Neuropathic symptoms, n (%)	2 (10.0%)	1 (16.7%)	12 (100%)	6 (100%)	<0.001
Pain, n (%)	0 (0%)	0 (0%)	4 (33.3%)	2 (33.3%)	0.014
Absence of ATR, n (%)	7 (35.0%)	6 (100%)	10 (83.3%)	6 (100%)	<0.001
Decreased vibratory sensation, n (%)	3 (15.0%)	5 (83.3%)	6 (50.0%)	5 (83.3%)	0.002
Abnormal NC in two or more nerve, n (%)	7 (35.0%)	6 (100%)	12 (100%)	6 (100%)	<0.001

Data are mean ± SD for age, BMI, HbA1c, duration of diabetes. Data are percentage for insulin treatment, retinopathy, nephropathy, neuropathy. NDR: non-diabetic retinopathy; SDR: simple diabetic retinopathy; PPDR: preproliferative diabetic retinopathy; PDR: proliferative diabetic retinopathy pain: one of small fiber neuropathy's sign; NC: nerve conduction; N: number of patients investigated by nerve conduction study.

Please cite this article in press as: Arimura A, et al. Intraepidermal nerve fiber density and nerve conduction study parameters correlate with clinical staging of diabetic polyneuropathy. Diabetes Res Clin Pract (2012), http://dx.doi.org/10.1016/j.diabres.2012.09.026

Table 2 – The neuropathological and neurophysiological findings of IENFD, CVR-R, NCS in diabetic polyneuropathy staging.

	Stage I	Stage II	Stage III + IV	Stage V	*p* values
IENFD (/mm)	13.8 ± 7.1	9.8 ± 15.2	3.0 ± 4.3	0.8 ± 1.3	<0.001
IENFD < 10/mm, % (*n*)	35.0 (7)	66.7 (4)	91.7 (11)	100 (6)	<0.001
CVR-R (%)	4.41 ± 2.65	3.09 ± 1.95	2.53 ± 1.64	1.33 ± 0.57	0.004
CVR-R < 2%, % (*n*)	10.0 (2)	33.3 (2)	33.3 (4)	83.3 (5)	0.001
Median CMAP (mV)	8.8 ± 3.8	6.9 ± 1.2	6.8 ± 3.1	4.8 ± 2.5	0.038
Median MCV (m/s)	53.2 ± 6.1	50.4 ± 4.3	48.6 ± 5.4	43.6 ± 5.4	0.006
Median F-wave latency (m/s)	26.1 ± 2.7	27.0 ± 4.5	28.7 ± 4.5	33.3 ± 1.2	0.007
Median SNAP (μV)	14.3 ± 19.1	6.6 ± 3.9	6.1 ± 2.2	2.7	0.044
Median SCV (m/s)	52.6 ± 7.4	37.7 ± 8.7	47.1 ± 5.3	42.6	0.002
Tibial CMAP (mV)	10.1 ± 3.7	7.2 ± 3.4	4.7 ± 2.6	2.7 ± 1.8	<0.001
Tibial MCV (m/s)	45.8 ± 3.8	44.8 ± 4.4	38.2 ± 4.7	34.6 ± 4.9	<0.001
Tibial F-wave latency (m/s)	47.3 ± 4.1	44.4 ± 2.5	52.1 ± 5.4	59.3 ± 3.3	<0.001
Sural SNAP (μV)	9.4 ± 5.0	6.7 ± 5.5	3.3 ± 2.3	3.9	0.013
Sural SCV (m/s)	48.3 ± 6.4	49.9 ± 6.4	42.0 ± 5.9	36.2	0.022

Data are mean ± SD for patients were stratified according to the neurological findings of IENFD, CVR-R, and NCS. Data are percentage for patients whose IENFD and CVR-R decrease. CMAP: amplitude of compound muscle action potential; MCV: motor nerve conduction velocity; SNAP: amplitude of sensory action potential; SCV: sensory nerve conduction velocity.

in stage II, 100% in stage III + IV, and 100% in stage V ($p < 0.001$).

The neuropathological and neurophysiological findings are shown in Table 2 and Fig. 1. Any complications were not occurred following the electrophysiological tests and skin biopsies were. A close association was observed between nerve function and DP staging as reported previously [12]. The IENFD was 13.8 ± 7.1 fiber/mm in stage I, 9.8 ± 15.2 fiber/mm in stage II, 3.0 ± 4.3 fiber/mm in stage III + IV, and 0.8 ± 1.3 fiber/mm in stage V ($p < 0.001$). The percentage of patients whose IENFD was below 10 fiber/mm (lower bound of 95% confidence interval in stage 1) were 30.0% in stage I, 66.7% in stage II, 91.7% in stage III + IV, and 100% in stage V ($p < 0.001$). One patient in stage II, two patients in stage III + IV, and five in stage V were not evoked SNAP of the sural nerve. Two patients in stage III + IV, and five in stage V were not evoked SNAP of the median nerve. We were unable to collect statistics for SNAP and SCV of the median and sural nerves, because five of six patients were not evoked in stage V. CMAP, MCV and SNAP of the median nerve and CMAP and MCV of the tibial nerve decreased with progressing stage and had close correlations with progressing stage. The F-wave latency of the median and tibial nerves was prolonged with progressing stage, and the differences were significant. CVR-R testing was analyzed in all patients. CVR-R decreased with progressing stage from 4.41 ± 2.65% in stage I, to 3.09 ± 1.95% in stage II, to 2.53 ± 1.64% in stage III + IV, and to 1.33 ± 0.57% in stage V ($p = 0.004$). The percentage of patients whose CVR-R was below 2% was 15.0% in stage I, 33.3% in stage II, 33.3% in stage III + IV, and 66.7% in stage V ($p < 0.001$).

We investigated the relationships between IENFD and diabetes-associated parameters (age, BMI, HbA1c, diabetes duration). No significant correlation was observed between IENFD and age ($r = 0.037$, $p = 0.811$), BMI ($r = 0.101$, $p = 0.514$), HbA1c ($r = -0.269$, $p = 0.077$), or diabetes duration ($r = -0.100$, $p = 0.517$).

The correlations between IENFD and NCS parameters are shown in Table 3. A significant correlation was observed between IENFD and CVR-R ($r = 0.399$, $p = 0.007$) and between IENFD and NCS parameters ($r = 0.378$–0.692, $p < 0.05$).

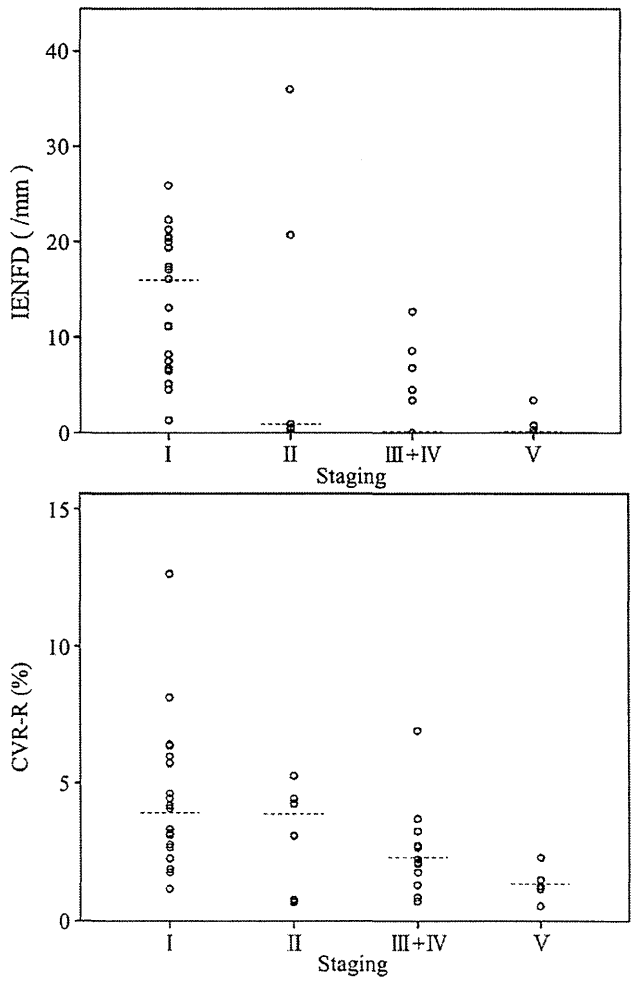

Fig. 1 – IENFD and CVR-R with the stage of diabetic polyneuropathy. A close association is observed between nerve function and the stage of diabetic polyneuropathy.

Please cite this article in press as: Arimura A, et al. Intraepidermal nerve fiber density and nerve conduction study parameters correlate with clinical staging of diabetic polyneuropathy. Diabetes Res Clin Pract (2012), http://dx.doi.org/10.1016/j.diabres.2012.09.026

Table 3 – The correlation of IENFD with NCS parameters.

	r_s	p values
Median CMAP	0.497	0.001
Median MCV	0.464	0.001
Median F-latency	0.5	0.001
Median SNAP	0.636	<0.001
Median SCV	0.486	0.002
Tibial CMAP	0.609	<0.001
Tibial MCV	0.599	<0.001
Tibial F-latency	0.492	0.001
Sural SNAP	0.692	<0.001
Sural SCV	0.378	0.023

Data are Spearman's correlations (r_s) and significance (p) between IENFD and NCS parameters. CMAP: amplitude of compound muscle action potential; MCV: motor nerve conduction velocity; SNAP: amplitude of sensory action potential; SCV: sensory nerve conduction velocity.

4. Discussion

The goal of this study was to validate the usefulness of clinical staging for DP using the criteria proposed by DNSGJ and findings of skin biopsy and NCS. We found that the neurological examination (IENFD, CVR-R, and NCS) significantly correlated with the progressing stage of DP. Our findings suggest that clinical DP staging reflects the progression of DP.

IENFD is reduced in patients with impaired glucose tolerance (IGT) and clinically overt diabetes [4,9,18], suggesting that epidermal nerves are affected in diabetes, and a skin biopsy is useful for evaluating small-fiber sensory neuropathy in patients with diabetes [18–21]. Our results concur with those of Quattrini reporting that IENFD decreases with increasing in severity of neuropathy and correlated significantly with the NCS parameters and CVR-R [21]. In contrast, Smith reported that IENFD does not correlate with clinical measures of neuropathy in patients with IGT and in patients with mild diabetes-associated neuropathy [9]. Previous studies have found that IENFD improves in patients receiving lifestyle intervention [22], in diabetic patients without DP [23], and in patients with post treatment painful neuropathy [24]. In other words, IENFD declines with IGT and early diabetic neuropathy and improves with the correction of glycemic control at the time of diagnosis of IGT and early diabetic neuropathy. In our study, IENFD varied widely among the patients in the early stage of neuropathy. For example, the ranges were 1.3–25.9 fiber/mm in stage I and 0–36 fiber/mm in stage II. These variations of IENFD were possibly due to the blood glucose fluctuation or rapid glycemic control observed in patients with early stage of diabetic neuropathy. Nerve fibers undergo degeneration and regeneration in patients with IGT and early neuropathy. However, once neuropathy progresses, degenerated nerve fibers do not regenerate. Our results show that IENFD decreased considerably in almost all patients subsequent to stage III, suggesting the marked decrease in IENFD was associated with advanced neuropathy.

The important risk factors for developing DP are hyperglycemia [25], diabetes duration [26], age [26], hypertension [27], smoking [27], height [28], level of alcohol consumption, and high cholesterol and triglyceride levels. We investigated the correlation between IENFD and risk factors for DP. IENFD was not associated with age, BMI, or HbA1c. Previous studies reported IENFD correlated with diabetic duration [20,29], but this study did not demonstrate the correlation between IENFD and diabetic duration. The diabetic duration might be incorrect because the onset of diabetes mellitus was sometime not clear, so some patients with severe polyneuropathy may already have complications of diabetes mellitus when they were given the diagnosis. IENFD was also not associated with height, hypertension, or high cholesterol and triglyceride levels. Although we examined a relationship between IENFD and risk factors for developing DP, the risk factors for developing small fiber neuropathy are not well understood. However, parameters related to metabolism, such as HbA1c, blood glucose, and cholesterol levels undergo significant changes with medical treatment; thus, IENFD may not be correlated with these metabolic parameters.

Pain and autonomic neuropathy are suggested small fiber neuropathy. Pain is an important symptom of diabetic neuropathy. Previous studies reported diabetic neuropathic pain was correlated with IENFD [30], automatic neuropathy [31] or contact heat-evoked potential (CHEP) [32,33]. Cardiac autonomic dysfunction and sudomotor symptoms are common components of diabetic autonomic neuropathy. The quantitative sudomotor axon reflex test (QSART) and sudomotor innervation in skin biopsy is used to assess sudomotor symptoms. Luo et al. showed the correlation of heart rate variability with sudomotor innervation [34]. Unfortunately, this study could not research CHEP, QSART and sudomotor innervation. In the future, the neuropathological and neurophysiological findings of diabetic neuropathic pain and sudomotor symptoms should be performed.

The known criteria for DP classify progressive neuropathy using special tests and equipment such as NCSs. However, these criteria are not practically available for clinicians, because NCSs are required special facility. A staging system with clinical neurological signs is required for many general physicians. Therefore, DNSGJ proposed simplified diagnostic criteria and clinical DP staging for daily practice. We showed that the diagnostic criteria and DP staging by DNSGJ reflected the results from IENFD, CVR-R and NCS parameters as a representative of small and large fiber neuropathy. In conclusion, our results indicate the usefulness of the DP diagnostic criteria and staging in clinical practice. It would be useful to further investigate whether the laboratory findings improve further and whether the treatment that fits each stage enables developing restraint.

The limitations of this study were as follows: the number of the patients in the present study is too small to complete multiple regression analysis, and we could not discuss the difference for staging of DP by DNSGJ in reautonomic neuropathy because the number of patients in stage IV with autonomic neuropathy was limited. This study is needed to continue and perform in more patients.

Conflict of interest

The authors report no conflicts of interest.

Please cite this article in press as: Arimura A, et al. Intraepidermal nerve fiber density and nerve conduction study parameters correlate with clinical staging of diabetic polyneuropathy. Diabetes Res Clin Pract (2012), http://dx.doi.org/10.1016/j.diabres.2012.09.026